A BRIEF LOOK INTO THE FUNCTIONALITY AND CAPABILITES OF SAGUARO, A DATA PROCESSING PLATFORM

OPTICAL METROLOGY PROCESSING WITH SAGUARO

ZACHARY J WALKER

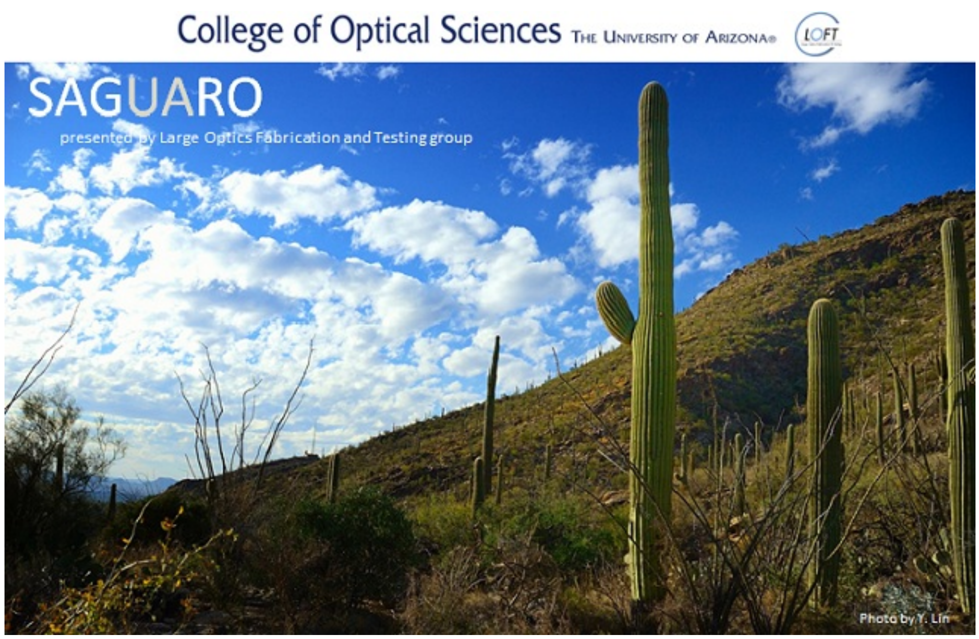

1.0 Abstract

The fabrication of an optical surface is only as good as its metrology. When topographical data is collected from a mirror or lens surface, effective processing stages must be analyzed for understanding surface error. SAGUARO provides a useful platform to analyze optical surface data. This report provides an overview of the functionality of SAGUARO, shown through use of processing tools called modules. The report will showcase optical surface data from the Daniel K. Inouye Solar Telescope (DKIST) 4.2-meter off-axis parabolic mirror. The data was collected during a two-week period of fine grinding. Through demonstrations of the software, the reader will have an understanding of how SAGUARO can aide an optical engineer or designer throughout optical surface fabrication and metrology.

Table of Contents

Table of Figures

List of Tables

2.0 Introduction

2.1 About SAGUARO

SAGUARO is an open-sourced software that was developed at the College of Optical Sciences, University of Arizona (http://www.loft.optics.arizona.edu). The Large Optics Fabrication and Testing (LOFT) group, comprising of faculty and students, developed the software. SAGUARO is a Matlab-based data processing platform that enables the manipulation and visualization of numerous data types. It is especially useful for data collected from optical testing equipment, such as profilometers, interferometers, deflectometers and laser trackers.

SAGUARO is an interactive platform hosting several modules to perform individual functions on specific formats of data. Modules are Matlab callback functions that allow the user to manipulate data through a graphic user interface. Often several modules are executed sequentially to obtain a desired outcome. SAGUARO provides a useful macro building section to easily string together modules for repeatability.

SAGUARO provides full integration with the user, allowing for modifications to standard modules, creation of custom modules, and personalization of configuration settings. SAGUARO continues to expand its module library by allowing users to submit their personal modules to be added to future software releases. Support using modules in SAGUARO is easily obtained by contacting the owner of the specific module, as their contact information is nested within the script.

2.2 About DKIST

The Daniel K. Inouye Solar Telescope (DKIST) is a current telescope project that when completed will mark the next generation ground-based solar telescopes (dkist.nso.edu). The project is divided amongst 22 institutions. The University of Arizona is one of those collaborators, and took the lead on fabrication of the 4.2-meter off-axis primary mirror. The nominal surface map is shown in Figure 1 (below).

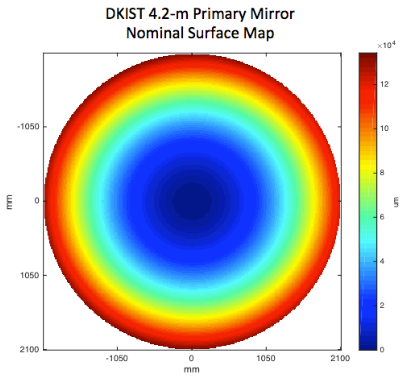

Figure 1 *DKIST 4.2 m off-axis primary mirror, nominal 2D surface map.*

2.2.1 Test Setup

To get a better understanding of the data used within the analysis, it is helpful to understand background information on the part under test, specifically the measurement technique used to acquire the datasets. The datasets used in this report have been collected and formatted at the University of Arizona. The mirror was measured using a novel IR deflectometery method developed at the University. This measurement technique directly measures local slopes, and provides highly accurate surface profiles of optical surfaces (Kim et al., 2015). Scanning Long-wave Optical Test Systems, or SLOTS, makes use of a thermal source to radiate long-wave radiation around 7-14 μm. Figure 2 (below) shows the test setup. These long wavelengths reflect off the ground surface of the mirror, and are collected by a thermal sensor. The SLOTS measurement states accuracy for ground-state optical surfaces with roughness varying from 0.7-1.6 μm rms (root-mean-square). The SLOTS method states 1 μm accuracy with a high spatial resolution (400x400 pixels), and large dynamic range (e.g. 9 mm departure over 4.2 m freeform optical surface).

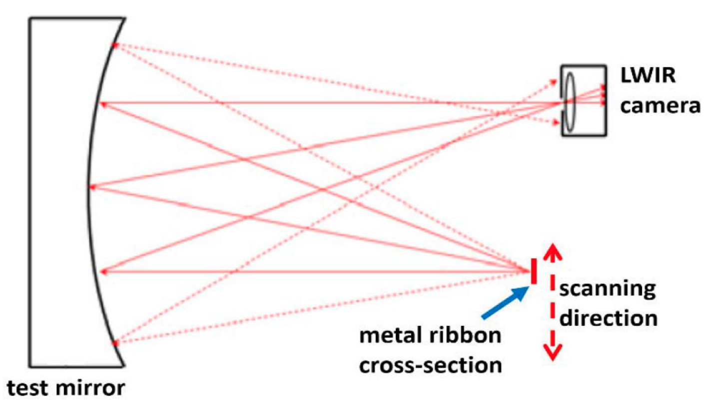

Figure 2 *SLOTS test setup*

2.2.2 Surface Error Maps and Tooling

A SLOTS measurement supplies a 2D rendering of the optical surface under test. The measured optical surface is subtracted from the nominal surface profile to give an error profile, or error map. Surface height error is defined in the same aspect as wavefront variance, where the error, or variance, is the departure from the ideal surface, or wavefront. The departure is then characterized through Zernike polynomials over the entirety of the optical surface. Surface figure errors, or surface aberrations, are referred to by the name of the fitted polynomials, i.e. coma, astigmatism, spherical, etc. The error map holds important information relating to surface figure and surface finish, two of the most difficult specifications to meet in the fabrication process and are the biggest cost drivers (Malacara, 2001).

The error map shows the departure from the ideal surface, and provides insight of the necessary removal for the proceeding grind run. The removal map is used with computer-controlled optical surfacing (CCOS) software to optimize material removal as a function of tool influence. Optical surfacing tools have removal properties that depend on their material composition, shape, applied pressure, compliance, and motion. All of these physical tooling variables are chosen by the optical engineer, and are integrated with CCOS software for simulating optical surfacing. Tools are designed based on features within the error map, and are modified as the surface shape changes.

The tool used on the DKIST 4.2-m primary mirror is a 0.6-m diameter Stressed lap, developed at the Steward Observatory Mirror Laboratory at the University of Arizona. The lap is computer-controlled, and permits its aluminum plate to conform at 100Hz, allowing for a close fit between the lap and the local optical surface (Kim et al., 2014). Due to the highly aspheric surface departure, a conformal tool of this nature is needed. The large size of the lap provides appropriate stiffness for smoothing as well as a large removal area to cut down on surfacing dwell times. This report analyzes a series of five surface error maps measured with SLOTS, over a two-week fine grinding span. The five surface error maps are shown in Figure 3 (below).

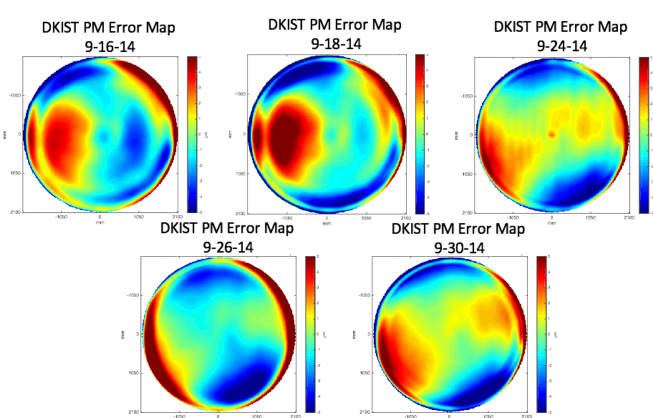

Figure 3 *Five DKIST primary mirror error maps over two week span, measured using SLOTS.*

3.0 SAGUARO Datasets

3.1 Types

Modules are functions that process data of a specific type. They commonly act upon six standard formats: *map, Zernike, freqmap, coordinates, layermap,* and *mask.* Each module will specify the input and output type that it is compatible with. If a foreign format is uploaded to SAGUARO, i.e. a *.mat* file from Matlab, the program has logic to convert the data to one of the six standard formats.

3.1.1 Map

The *map* data types are two-dimensional matrices that contain data for surface profiles, optical path differences, or interferograms. These contain real values, for purposes of arithmetic and plotting, and may also contain NaNs (not-a-number) to indicate masked regions. The main use of this data type is for error analysis of optical surfaces. Surface error maps show the departure from the nominal, or prescribed optical surface. They show the progression of an optical surface as it is ground or polished during fabrication. Surface error maps are used to quantize surface irregularity in terms of height discrepancy. For surfaces with a circular aperture, Zernike polynomials are used to quantize the error.

3.1.2 Zernike:

The *Zernike* data types hold Zernike coefficients. SAGUARO uses the same Zernike notation as Zemax in terms of relating coefficients to polynomials, i.e. $a_1 Z_0^0 + a_2 Z_1^{-1} + a_3 Z_1^1 + a_4 Z_2^0 + a_5 Z_2^{-2} + a_6 Z_2^2 + \cdots a_j Z_n^m$. (See Appendix A for more on Zernike notation.) The dataset is a three-column matrix. The first column specifies the Zernike coefficients, the second column specifies the azimuthal degree *m*, and the third column specifies the radial degree *n*. Table 1 (below) shows the proper formatting of this data type.

Zernike Coefficients [μm]	m	n
4E-06	0	0
0.05E-06	1	1
0	-1	1
0	0	2
-1.34E-06	-2	2
1.76E-06	2	2

Table 1 *Zernike coefficients with corresponding indices, demonstrating proper SAGUARO Zernike format.*

Error from optical surfaces with circular apertures, is quantized through Zernike coefficients, due to the continuous and orthogonal behavior of Zernike polynomials. Using the normalized Zernike expansion to describe aberrations offers the advantage that the coefficient, or value of each mode, represents the rms wavefront error attributable to that mode (Fleck et al., 2011). Quantizing Zernike coefficients directly relates to surface figuring, or the arrangement of the surface errors. Having an understanding of the dominant surface error, through use of Zernike polynomials, allows for precise correction of the surface figure through proper tooling and CCOS.

3.1.3 Freqmap:

The *freqmap* data type is a Fourier transform of a spatial surface map. It is a matrix of complex values representing spatial frequencies existing in an optical surface. These datasets are outputs from a module that performs a Fourier transform of the input data. A use of this data type is spatial frequency filtering, where desired frequencies are filtered, or removed from the *freqmap*. An inverse Fourier transform is taken to reconstruct the optical surface, without the filtered spatial frequencies. (See sections 4.1.3 – 4.1.5 for an example of this process.)

3.1.4 Coordinates

The *coordinates* data type is a matrix specifying spatial coordinates, for example Cartesian or polar coordinates, with each column of the matrix representing a spatial component (i.e. x/y/z or ρ/z). Optical surface data is acquired by spatial sampling with one of the aforementioned metrology devices. These devices produce a set of spatial coordinates representing the optical surface, which is exported in either Cartesian, polar, or spherical components. One use of this data type is reconstructing surface maps, from sampled optical surface data. Upon converting to a surface map using SAGUARO, various processing can be done for further analysis.

3.1.5 Layermap:

The *layermap* data types are maps, or matrices, that hold several layers of information, such as gradients. One use of this data type is deflection analysis of rigid materials, where the *layermap* is used as a nodal deflection matrix, made up of the various deflection components μ_x, μ_y, μ_z. Though useful for finite element analysis applications, this data type is outside the scope of this report, and thus none of the modules discussed will call upon it.

3.1.6 Mask:

The *mask* data types are matrices containing 1's and NaNs that are used to mask regions of interest. They are applied to surface maps for uses of removing bad data and for resizing maps. Masking excludes regions of a dataset for analytical purposes. One example shows masking features in a surface map that may be driving the slope magnitude rms high. This allows a prediction of the surface statistics once the bad data is corrected through optical surfacing.

4.0 Standard Modules

The current release of SAGUARO (version 1.6.5) comes with over 30 preloaded, standard modules. These standard modules continue to grow, as LOFT encourages user-submissions.

SAGUARO has four module categories: conversion, general, plotting, and custom. Each category is highlighted, providing an explanation of each module, as well as a demonstration if applicable to optical metrology. The modules will operate on data from the DKIST primary mirror, data provided from SAGUARO, and simulated data.

It is important to note that each module has an associated help file. This file provides a brief explanation of the functionality of the module, as well as the input and output data types. For questions related to the module, the help file also contains the contact information for the creator of the module.   An example of a help file is shown in Figure 4 (below), and corresponds to the first module under review.

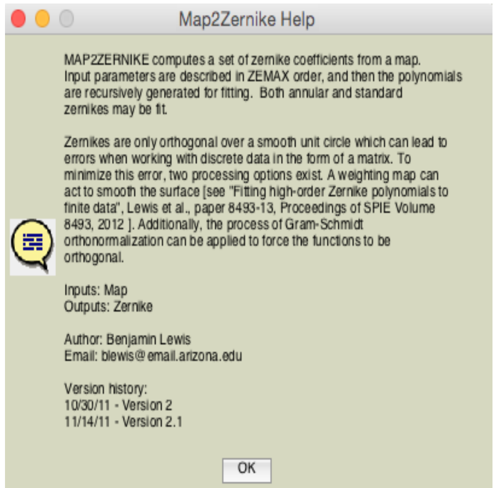

Figure 4 *Help prompt for Map2Zernike module.*

4.1 Conversion Modules

The modules under the conversion category are: *Map2Zernike, Zernike2Map, MapFFT, FreqMapIFFT, PSD, RadiallyAvg2Coords, CoordinatesPlot, RadCoords2Map, Coordinates2Map, StructureFunction, UnitConvert, and GenDataConvert.* All of these modules perform conversion operations, where the output data type is different from the input data type.

4.1.1 Map2Zernike

Map2Zernike decomposes a surface map into a set of Zernike coefficients. They are defined by either standard or annular Zernike polynomials, dependent of the surface map. The user chooses the number of Zernike terms for fitting. Figure 5 (below) shows an example of fitting the first eleven Zernike polynomials to an astigmatic surface map (provided within SAGUARO's documentation). The astigmatic terms are z5 = z6 = 1.3 µm.

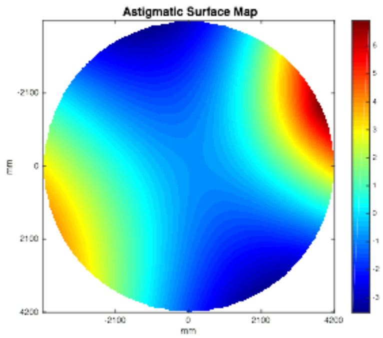

z [µm]	n	m
0	0	0
0	1	1
0	-1	1
0.39	0	2
1.329	-2	2
1.253	2	2
0.047	-1	3
0.093	1	3
0.338	-3	3
0.117	3	3
-0.038	0	4

Figure 5 *Astigmatic Surface Map (left), and corresponding table of Zernike coefficients over the first 11 terms, produced from Map2Zernike.*

4.1.2 Zernike2Map

Zernike2Map works in the exact opposite as *Map2Zernike*. With this module a Zernike prescription is input in terms of Zernike coefficients, and then SAGUARO recursively generates the corresponding surface map. Figure 6 (below) shows a reconstructed comatic surface map from Zernike coefficients z7 = z8 = 0.05 µm. The module allows the user to specify the number of pixels to construct the map. This module can be used in surface design, as well as a learning tool for visualizing aberrations in 2D.

z [µm]	n	m
0	0	0
0	1	1
0	-1	1
0	0	2
0	-2	2
0	2	2
0.05	-1	3
0.05	1	3
0	-3	3
0	3	3
0	0	4

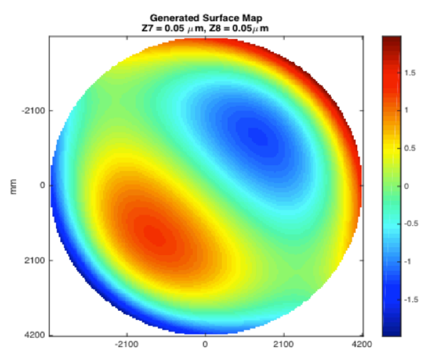

Figure 6 *Zernike coefficient prescription (left), corresponding generated surface map (right), produced using Zernike2Map module.*

4.1.3 MapFFT

MapFFT performs the Fourier transform of a 2D surface. It uses Matlab's *fft2* function that performs the fast Fourier transform of a 2D object. Figure 7 (below) shows the module executed on a DKIST surface error map. Converting from the spatial domain to the spectral domain, allows for frequency analysis, such as frequency distribution or frequency filtering.

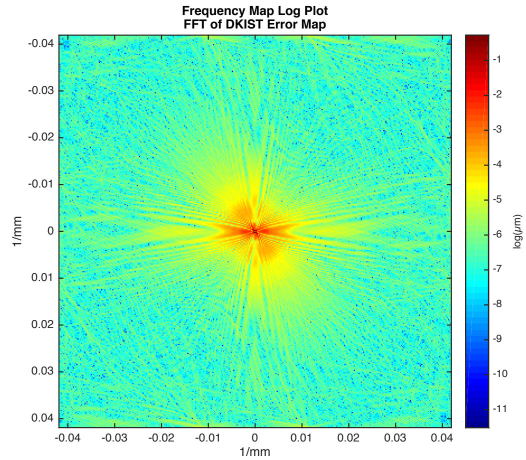

Figure 7 *Log plot of the Fourier transform of a DKIST error map, using module MapFFT*

4.1.4 FreqMapIFFT

FreqMapIFFT performs the inverse Fourier transform on a frequency map. This module is useful for plotting a spatial map after frequency filtering. Figure 9 (below) shows a low-pass filtered map from the example, with a cutoff frequency 0.0025 mm^{-1}. The filtered map shows a sharp ringing effect, which is not expected for a low pass filter. This is likely an effect from the type of frequency filter used. The frequency response using *FreqMap_LPFilter* corresponds to a circle function with a sharp edge defining the cutoff in the frequency domain. Therefore, its corresponding inverse Fourier transform is that of a Bessel function, hence the ringing effect in the spatial domain (Rao et al., 2010).

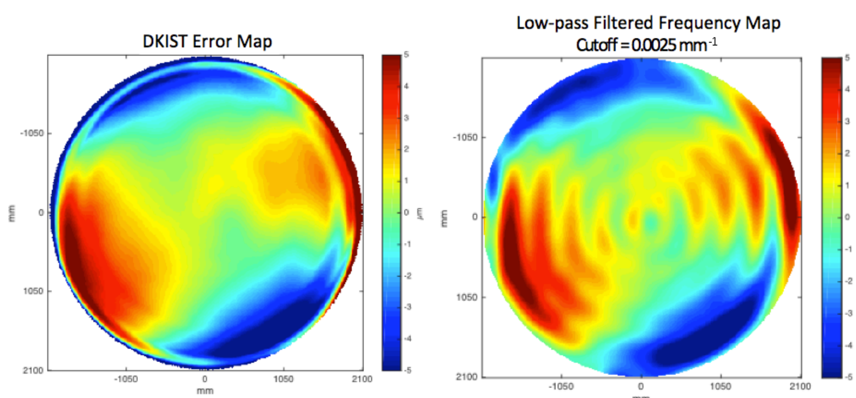

Figure 8 *Unfiltered DKIST surface error map (left), and filtered with cutoff frequency 0.0025 mm^{-1} (right).*

4.1.5 PSD

PSD calculates the 2D power spectral density of the input map. It is defined by the product of the Fourier transform with the complex conjugate of the Fourier transform, divided by the area of the optical surface. When an optical surface has a circular aperture, the PSD is used to characterize the mid- and the high-spatial frequency components of its surface height (Sidick, 2009). In the case of circular apertures, Zernike polynomials are used to analyze the low frequency surface figure. The PSD is able to provide an analysis of the surface quality for optical surfaces without a circular aperture, in place of Zernike polynomials. Figure 10 (below) shows the PSD of a DKIST error map.

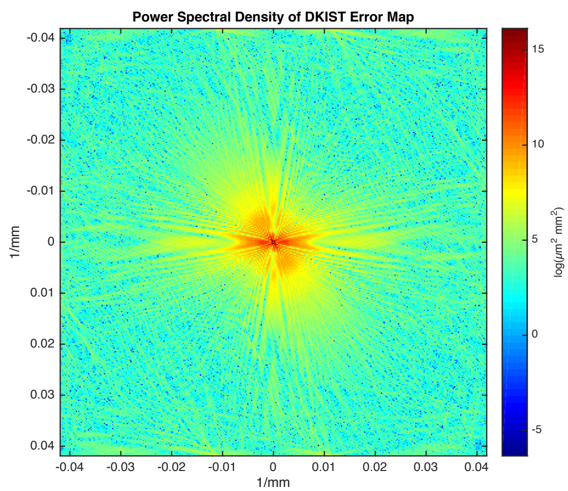

Figure 9 *PSD of DKIST surface error map.*

4.1.6 RadiallyAvg2Coords

RadiallyAvg2Coord performs a radial average of a 2D map, generating polar coordinates in ρ and z. Upon generating the coordinates, a plotting module becomes accessible, called *CoordinatesPlot*, allowing the user to plot z vs. ρ. Figure 11 (below) shows the radially averaged profile of the nominal DKIST surface map, which displays the parabolic surface profile. This module is useful for representing 2D radially symmetric surface maps as profiles. This module is also useful for tracking radially averaged error over time.

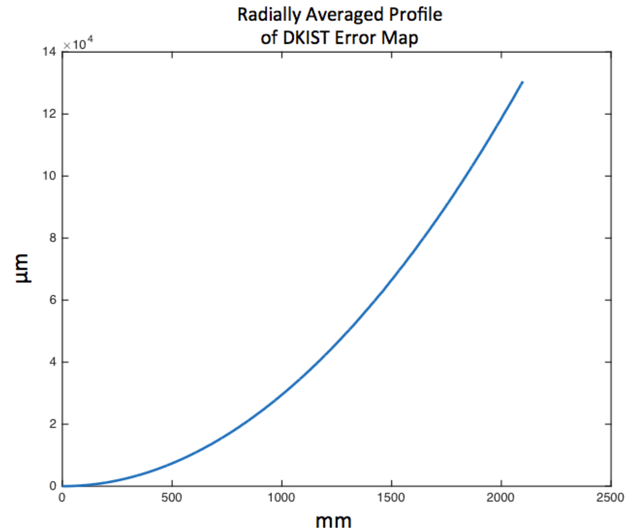

Figure 10 *DKIST radial surface profile generated by RadiallyAvg2Coords and CoordinatesPlot.*

4.1.7 CoordinatesPlot

CoordinatesPlot plots 2D and 3D data of type *Coordinates.* The outputs are plot, trimesh, gridmesh plot, or surface plot. This is the go to module for plotting once data is uploaded in the *Coordinates* format.

4.1.8 Coordinates2Map

Coordinates2Map coverts data sets of type *Coordinates,* that have three columns of data, to *Map* data types. The data is assumed to be in the order X, Y, Z respectively. Upon running the module, the desired size of the matrix is requested in pixels.

4.1.9 RadCoords2Map

RadCoords2Map reconstructs a map with a given dataset in the form of radial coordinates, i.e. ρ and θ. The module asks for the desired size in pixels to reconstruct over.

4.1.10 StructureFunction

StructureFunction computes the structure function of a surface map. The structure function provides an alternative specification for surface irregularity, aside from surface rms and surface P-V. The module computes rms height as a function of physical separation between surface points.

The module plots a logarithmic or linear plot of the rms values as a function of the separation distance.

Modern optical fabrication methods employ undersized polishing tools, generating irregularities on sub-aperture scales or mid-spatial frequencies (Zhelem, 2011). Improper use of tooling affects the fabrication of aspheric or free form surfaces. The smoothness of local polishing depends entirely on how the tool influences removal on a surface. The tool must have a controlled influence, as well as a controlled dwell time. The structure function performs a more adequate means of characterizing irregularity due to mid-spatial frequencies (Zhelem, 2011). Figure 12 (below) shows the structure function of a DKIST surface error map, represented by a log-log plot.

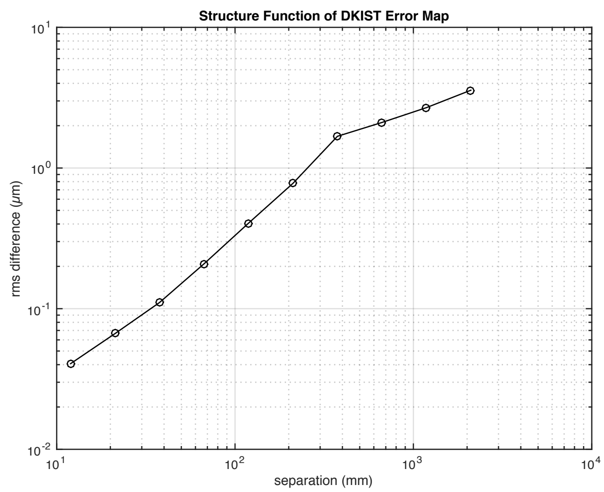

Figure 11 *Structure function of DKIST error map from 9/30/14.*

4.1.11 UnitConvert

UnitConvert allows the user to selectively change the units of any column within a dataset (i.e., millimeters to micrometers, millimeters to inches, or any custom conversion). Being able to change units is desirable for plotting purposes, as well as displaying statistical values in the desired units.

4.1.12 GenDataConvert

GenDataConvert is a module that converts foreign datasets into SAGUARO preferred formats. This allows many outside datasets to be used with the program. Figure 12 (below) shows the prompt when the module is ran, asking the user to select the desired conversion format.

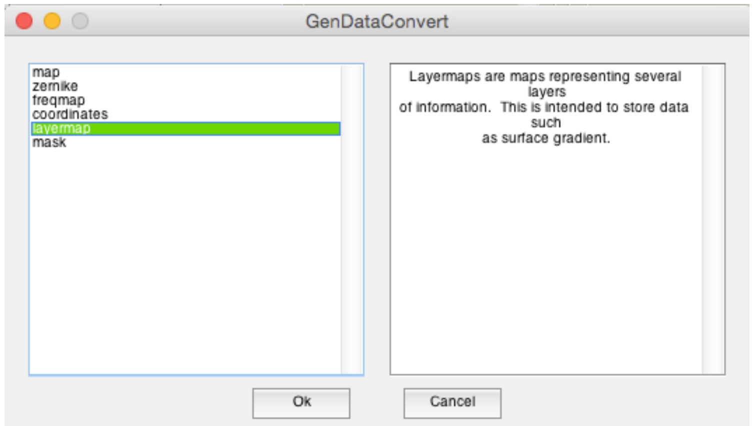

Figure 12 *GUI for converting data between data types*

4.2 General Modules

The modules under the General Modules category are: *ApplyArbitratyFunction, BadDataRemoval, FlipX, FlipY, FlipZ, MapArithmetic, MapMaskTool, MapMedianFilter, FreqMap_LPFilter, FreqMap_TukeyFilter, MapRotate, MapValueReplace, MaskBadData, TrimData, ZernikeTermRemoval, Zeropadding, AveragedDatasets, and MapCombine.* These modules are used for data manipulation and analysis.

4.2.1 ApplyArbitraryFunction

ApplyArbitraryFunction allows the user to apply any Matlab-based function to the input. It works for all SAGUARO data types. Figure 13 (below) shows the cosine of a surface map. The cosine is equivalent to the sum of the Taylor series expansion: $I - \frac{A^2}{2!} + \frac{A^4}{4!} - \frac{A^6}{6!} + \frac{A^8}{8!} - \cdots$, where A represents the surface map, and I represents the identity matrix of equal size. Taking the cosine of a surface map shows relative phase shifts between pixels in the surface map, and is shown in Section 7.1 how this is applicable towards simulating interferograms.

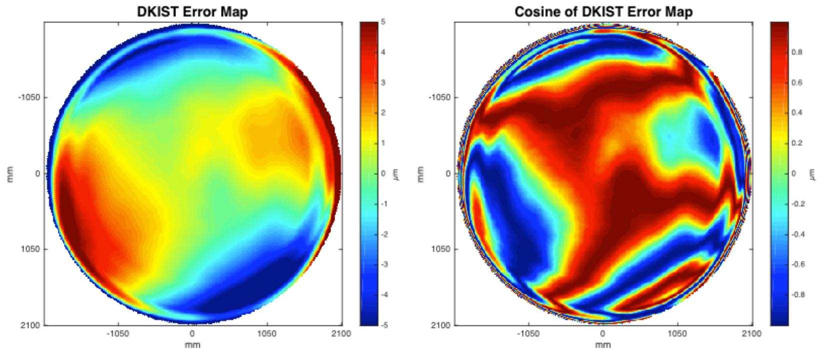

Figure 13 *DKIST error map (left), and cosine of the error map (right).*

4.2.2 BadDataRemoval

BadDataRemoval provides an interactive method of selecting unwanted artifacts for removal. Artifacts arise from many reasons, including measurement and surface reconstruction. The module allows the user to interactively select regions containing bad data, and then interpolates those regions to fill the voids. Figure 14 (below) shows an example of the module, where the user selects defects (left), and the post processed map (right).

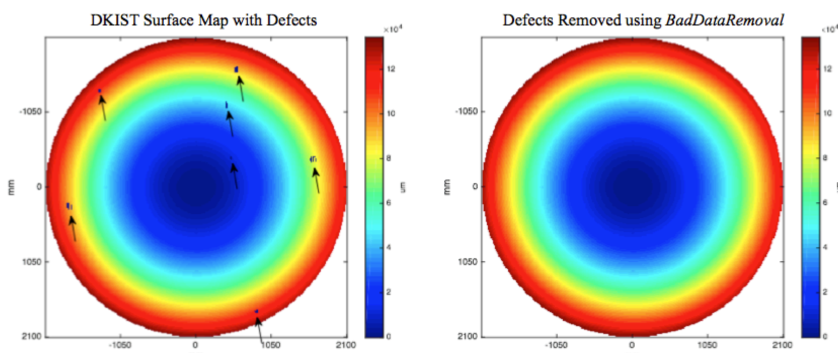

Figure 14 *DKIST surface map with added defects (left), filtered map using BadDataRemoval (right).*

4.2.3 MapMaskTool

MapMaskTool allows a dataset to be masked with a variety of geometries. A GUI allows the user to upload a desired mask, or use the built-in circular mask option to specify the inner and outer diameter of the mask. This module works well in conjunction with other modules that may lose the desired geometry of the dataset. This module can be applied to surface maps for uses of masking bad data, as well as for analyzing surface statistics over masked regions. Figure 15 (below) shows an annular mask applied to a surface map, with specified inner and outer radii.

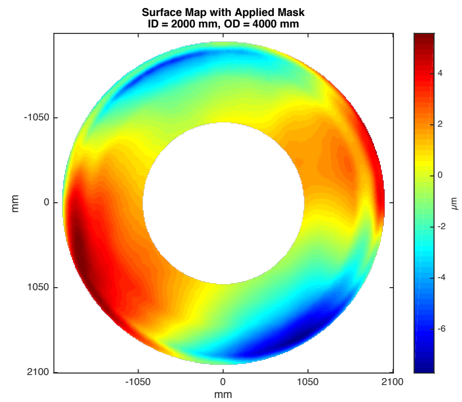

Figure 15 *Annular mask applied to DKIST error map.*

4.2.4 FlipX, FlipY, FlipZ

The modules *FlipX, FlipY, and FlipZ* switch the sign across the desired axis. This is helpful with incorrect orientations due to data formatting and stitching. Figure 16 (below) shows an annular surface map flipped across each axes.

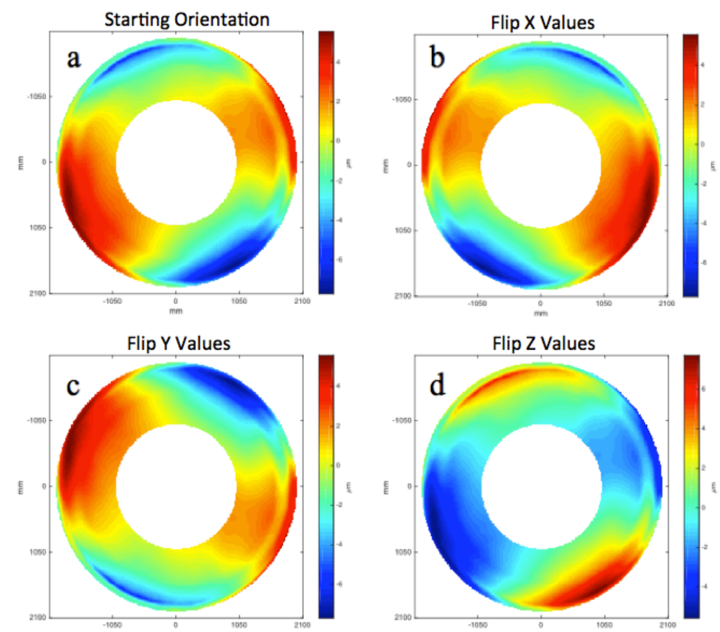

Figure 16 *Applying coordinate sign changes to a surface map (a) about the x-values (b), the y-values (c) and the z-values (d).*

4.2.5 MapArithmetic

This module allows the user to manipulate the dataset with basic operators (i.e. addition, subtraction, multiplication, and division). This module provides quick scaling of datasets. In one example, show in Figure 17 (below), it is used to scale removal maps used in polishing and figuring optical surfaces. Scaling the magnitude of a removal map gives an optical designer the ability to adjust dwell times, targeting specific percentages of desired removal.

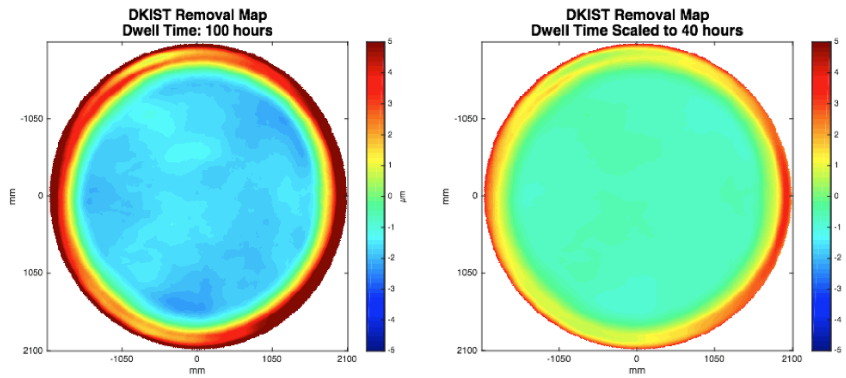

Figure 17 *DKIST surface removal map (left), and 40% scaled surface removal map (right).*

4.2.6 MapMedianFilter

MapMedianFilter applies a common median filter to the dataset. The user chooses the desired kernel size for which the median filter works over. This module is ideal for datasets with defects or noisy data, providing quick filtering. This module is susceptible to removing desirable high spatial features, i.e. edge effects, if the kernel is too large.

4.2.7 FreqMap_LPFilter

FreqMap_LPFilter applies a radial mask to a frequency map, such that only frequencies within the masked region remain. The user defines the cutoff frequency, such that all frequencies lower will pass. The cutoff frequency defines the radius of the masked region. The map in Figure 18 (below) shows an example of this module used on the frequency map from Figure 7 (above). The cutoff frequency is set to 0.025 mm^{-1}. This module only applies the circular filter; an inverse Fourier transform must be performed in order to return spatial coordinates.

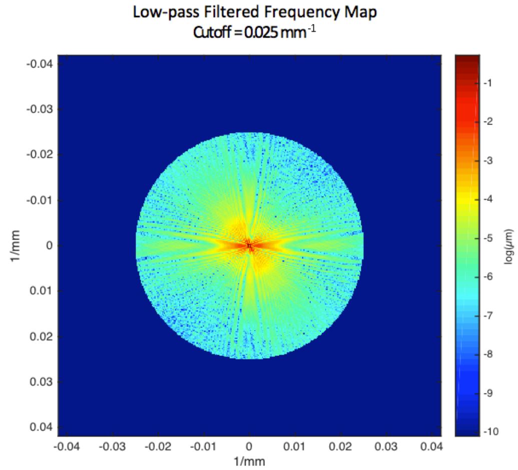

Figure 18 *Filtered frequency map, cutoff = 0.025 mm*$^{-1}$.

4.2.8 FreqMap_TukeyFilter

FreqMap_TukeyFilter applies a spatial frequency filter to a *Freqmap* data type. The filter specifies a spatial frequency cutoff, as well as a ratio of the constant section to the filter size (0<=ratio<=1). The filter tapers to 0.5 at the cutoff frequency. Figure 19 (below) shows an example of a Tukey filter used on the *freqmap* from Figure 7 (above).

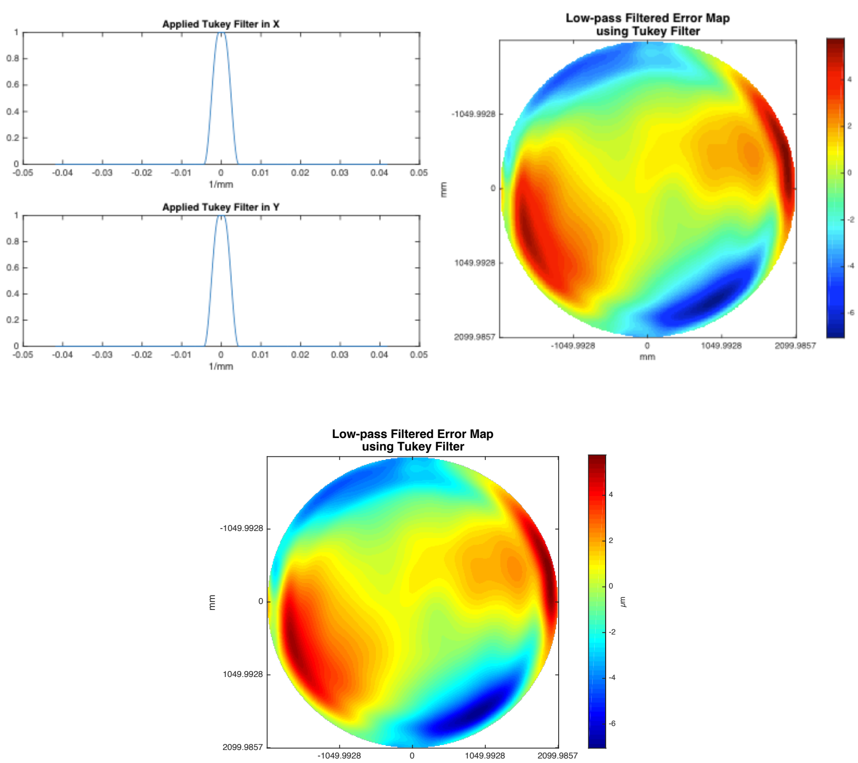

Figure 19 *Example of Tukey Filter (top), and resulting map (bottom). Cutoff frequency = 0.0025 mm*$^{-1}$.

4.2.9 MapRotate

MapRotate simply rotates a dataset based on the input angle in degrees. It uses the notation of negative angles represent counterclockwise rotation, and positive angles represent clockwise rotation. Because matrices are rectangular, the user has the option to preserve the original dataset size by selecting a trimming option.

4.2.10 MapValueReplace

MapValueReplace substitutes any user-specified value with NaNs. SAGUARO uses NaNs commonly with formatting, making this module ideal for converting a foreign data type to an alternate format.

4.2.11 MaskBadData

MaskBadData provides the ability to select a region of data on a surface map to mask. The module can either keep what is inside or outside of the mask. The selected region is either an ellipse, or a polygon. The example shown by Figure 20 (below) demonstrates the polygon feature selecting an arbitrary region to mask, and removes all the data within.

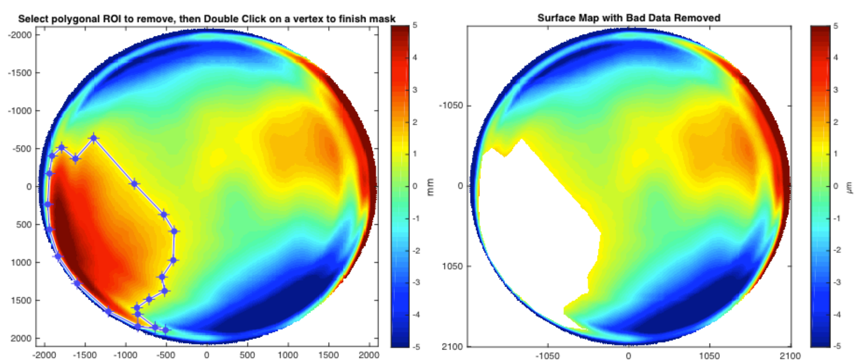

Figure 20 *Using polygon removal feature of* MaskBadData.

4.2.12 TrimData

TrimData removes excessive NaNs from matrices. Maps may acquire excessive amounts of NaN-values, caused from modules that replace real values with NaNs, such as masking tools. Excessive NaNs alter the effects of other modules, such as Zernike term fitting and removal. The module provides flexibility in how much data are trimmed, and whether the dataset remains centered.

4.2.13 ZernikeTermRemoval

ZernikeTermRemoval removes desired Zernike polynomials from a surface map. It can remove either annular or standard Zernike polynomials, depending on the map type. The example shown in

Figure 21 (below) removes astigmatism Zernike polynomials, z5 and z6, from the astigmatic surface map.

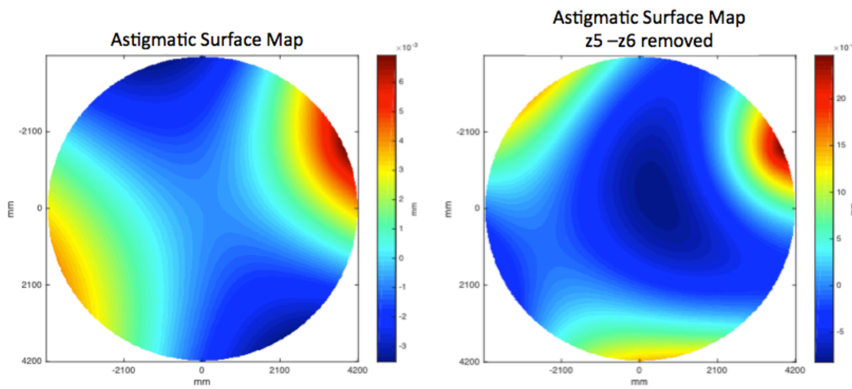

Figure 21 *Astigmatic Surface Map (left), Astigmatic Surface Map with Z5, and Z6 removed (right)*

Removing dominating aberration reveals remaining high-order aspheric modes. This module is applicable in two approaches. The first approach as just shown, removes aberrations with the largest magnitudes in order to reveal modes of lower impact. On the contrary, the second approach involves removing the low magnitude modes in order to pronounce dominating features. For either case, this module provides quick qualitative assessment of both high and low magnitude features.

It is common practice to remove alignment modes x-tilt (z2), y-tilt (z3), and focus (z4) from optical surface measurements. Alignment refers to the object under test relative to the test instrument, where each object point has three degrees of freedom, x, y and z (Malacara, 2007). Because these terms are alignment artifacts and do not contribute to real surface figure they are removed. Removing these terms is important when comparing one dataset to another, as it removes bias from the testing instrument.

4.2.14 ZeroPadding

ZeroPadding pads the input dataset by the specified radial amount with zeros. Zeropadding is desirable for increasing the sampling rate of a discrete Fourier transform (DFT). This technique allows the DFT to approach the continuous Fourier transform (CFT), as the length of the padding increases. When we sample a continuous time-domain function, and take the DFT of those samples, the DFT results in a frequency-domain sampled approximation of the CFT (Lyons, 2011). As the DFT increasing in sample size it approximates the CFT. This principle is applied to discrete sampling of an optical surface. A theoretical continuous optical surface is discretized by both measuring resolution, and down sampling in data formatting. By applying the same zeropadding method to optical surface data, a more accurate spectral estimation is achieved when performing the DFT. Figure 22 (below) showcases the effect of zeropadding a comatic surface map with minimal sampling (17x17 pixels). The example shows the clear correlation of increased padding to increased resolution, or sampling, in the frequency domain.

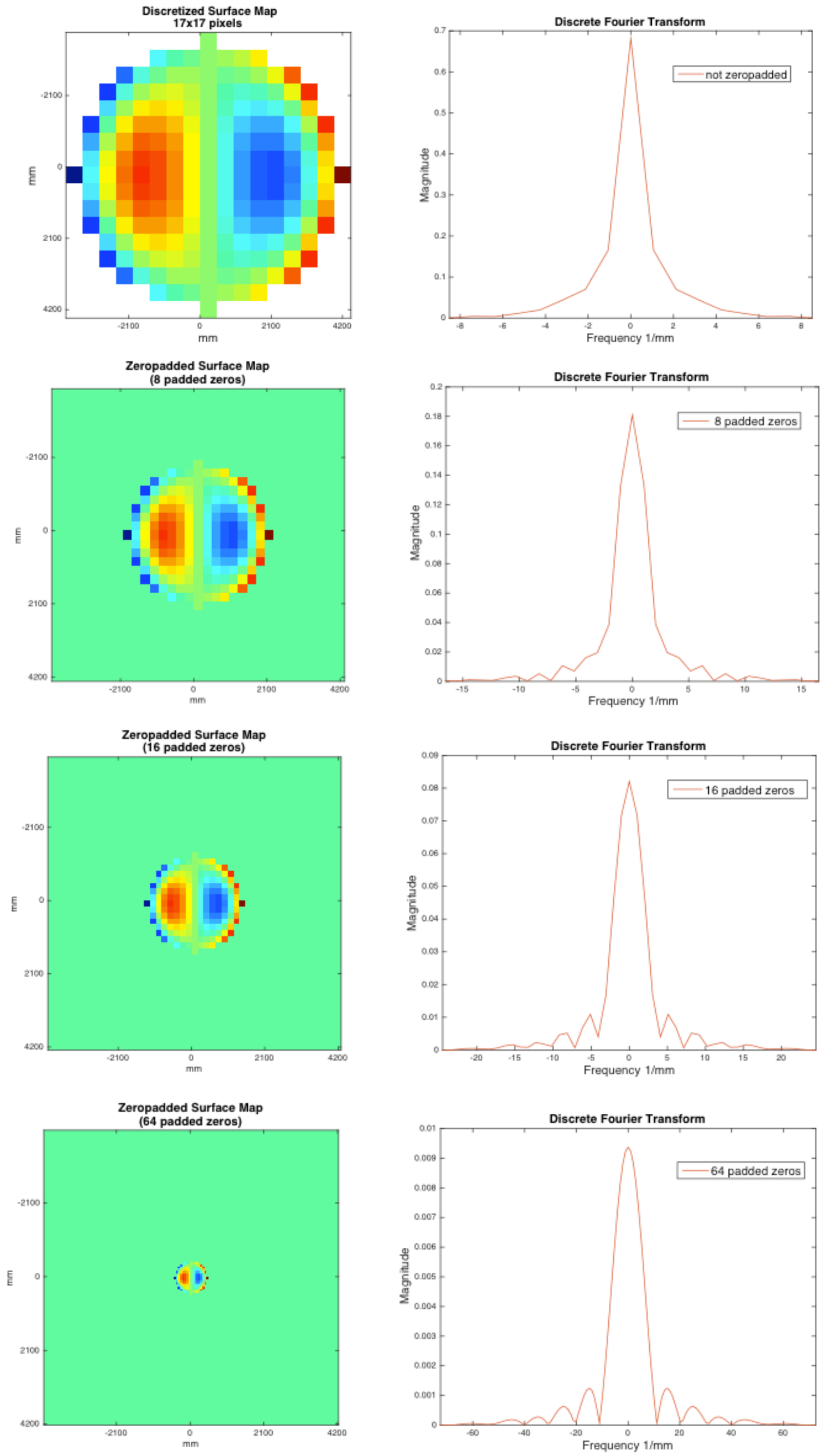

Figure 22 *Example of zeropadding to achieve higher resolution in the frequency domain. No padding (first row), 8 padded zeros (second row), 16 padded zeros (third row), 64 padded zeros (last row).*

4.2.15 AverageDatasets

AverageDatasets performs a pixel-by-pixel average of datasets of various formats, i.e. maps, masks, and freqmaps. Two or more input datasets must be highlighted for this module to become available. The datasets must have the same properties for this module to work. The output is a single dataset with the same properties of the input datasets. This is a useful module for averaging many datasets over an extending period of time, i.e. analyzing surface map error through averaging.

4.2.16 MapCombine

MapCombine allows two maps with identical size to be manipulated with basic operators, i.e. addition, subtraction, division, multiplication. This module is very useful when comparing consecutive measurements, as this shows the change between the two. Applything this to optical surfacing, we can compare consecutive error map measurments to see the measured removal between the two. This allows an optical designer to compare the measured removal to the predicted removal. Comparing the predicted vs. measured removal shows the optical designer how the tooling simulation can be adjusted (i.e., scaling the Preston's Constant). Figure 23 (below) shows this module is use, where dataset 2 is subtracted from dataset 1 for a resulting difference map.

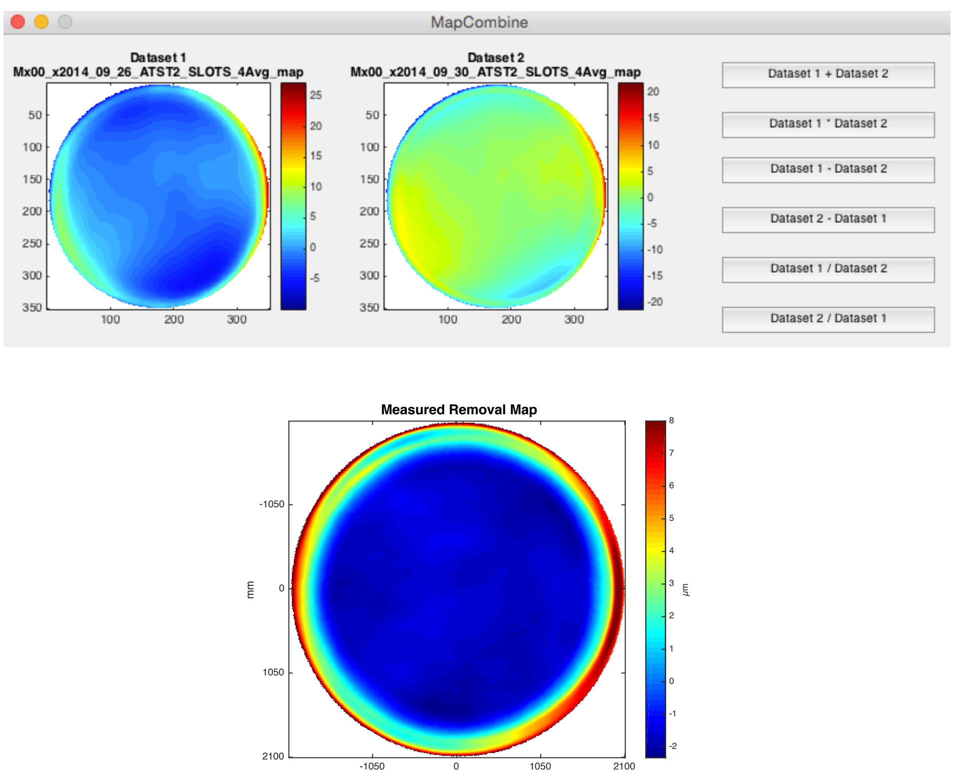

Figure 23 *MapCombine GUI and resulting difference map.*

4.3 Plotting Modules

The third module category is *Plotting*, and contains only four modules: *MapContourPlot, MapPlot, MapStatistics, and FreqMapLogPlot.*

4.3.1 MapContourPlot

MapContourPlot displays a 2D dataset as a contour map, where the user specifies the number of contour levels. One application of this module is mapping dominant features within an error map. If desirable, opticians can hand polish surface errors and not rely on CCOS. For large optics, opticians can draw on the optical surface with marker, to indicate regions for correction and to provide a guideline for their tool. Opticians can easily mark these features while the part in under an optical test, as the live interferogram acts as a coordinates plot showing exact regions of error. This module acts in the same sense, as it provides mapping and coordinates of dominate features. Figure 24 (below) converts an error surface map to a contour map.

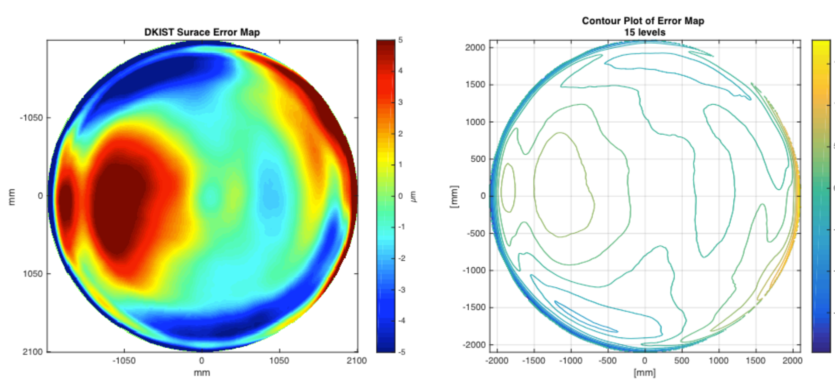

Figure 24 *DKIST error map 9/18/14 (left), corresponding contour map with 15 levels (right).*

4.3.2 MapPlot

MapPlot produces an image of a map dataset using the Matlab command: *imagesc*. It is one of the most basic, yet most used SAGUARO modules.

4.3.3 MapStatistics

MapStatistics provides statistical analysis of the input map, as well as displays various slope plots. The module computes the surface rms, surface P-V, and slope magnitude rms. The module displays slope maps along the x-directions, y-directions, tangential zones, and radial zones.

The two most difficult to meet specifications in the fabrication processes, are surface figure (macrotopography) and surface finish (microtopography) (Malacara, 2001). Surface figure is specified by surface rms, or surface peak-to-valley (P-V), where both denote the height disparity between the measured and nominal optical surface. These values are listed in spatial lengths, or more commonly in waves, i.e. 0.16 µm or 0.25 wave, where the wavelength used for conversion is the wavelength used to test the optical part. Typical figure tolerances are 0.2 to 0.05 waves rms at the measurement wavelength of the HeNe laser at 632.9 nm (Malacara, 2001).

Aspheric surfaces will have slopes that vary between a few micrometers, and few tens of micrometers, over the diameter of an optical surface, depending on how strong the aspheric departure is. Large surface slopes can contribute to tool misfit over local regions, i.e. if a tool is too large to fit local slopes, tool wear may occur in undesired zones, creating sharp features that are difficult to get rid of (Malacara, 2001). Proper tooling, in terms of size and compliance, is required for preventing and fixing these unwanted zones. Plotting slope maps allows for identification of sharp features and zones. Figure 25(below) shows the slope coordinate system for the slope maps generated with this module. An example of this module performed with a DKIST error map is demonstrated by Figure 26 (below) and Figure 27 (below).

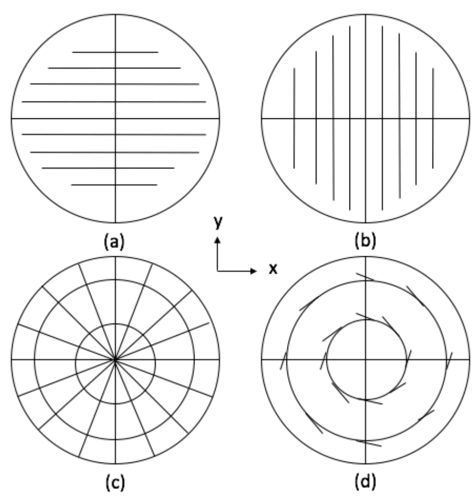

Figure 25 *Slope maps along various directions. Along x-directions (a), y-directions (b), radial zones (c), tangential zones (d).*

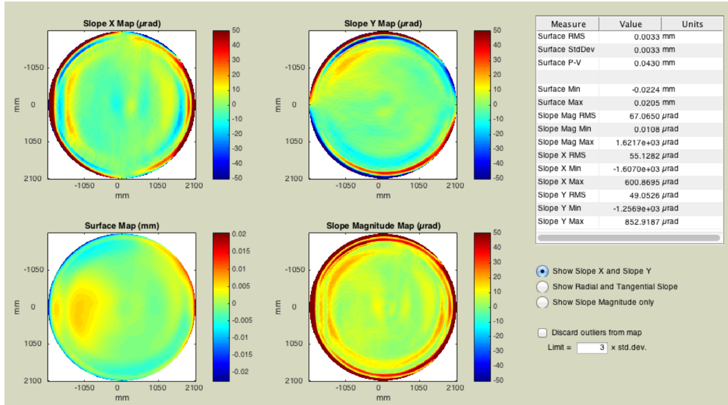

Figure 26 *Slope maps along x-directions and y-directions, as well as slope magnitude map and surface statistics.*

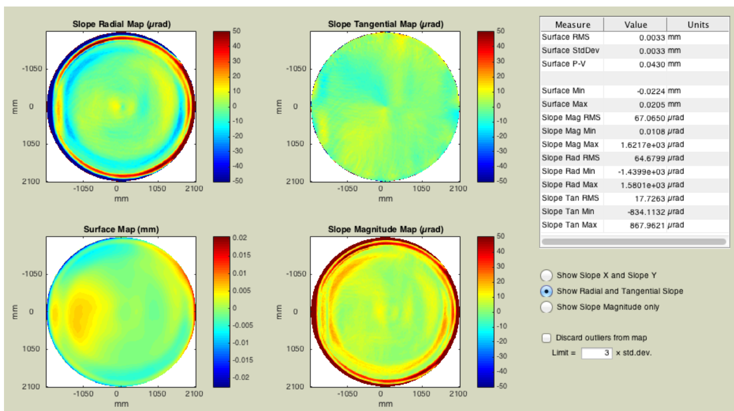

Figure 27 *Slope maps along radial directions and tangential directions, as well as slope magnitude map and surface statistics.*

4.3.4 FreqMapLogPlot

FreqMapLogPlot plots the log of a *freqmap* data type using the Matlab command imagesc.

5.0 User Modules

SAGUARO allows the user to create personal modules. The software provides a template script within its documents, to demonstrate the standard format, making it simple for the user to get started. User modules follow all of the same guidelines as the standard modules, i.e., dataset types and formatting. This section highlights two user modules that are applicable to optical metrology.

5.0.1 HighPassLowPass

HighPassLowPass module achieves frequency filtering by performing a convolution of the input map with a 2D Gaussian kernel. The standard deviation and kernel size of the Gaussian is user-specified in the configuration file. This module produces four plots, shown in Figure 28 (below): the input map, the kernel used, as well as the low-pass and high-pass filtered maps. Both filtered maps are then exported and have the option to be saved. This module provides SAGUARO with additional means of frequency filtering.

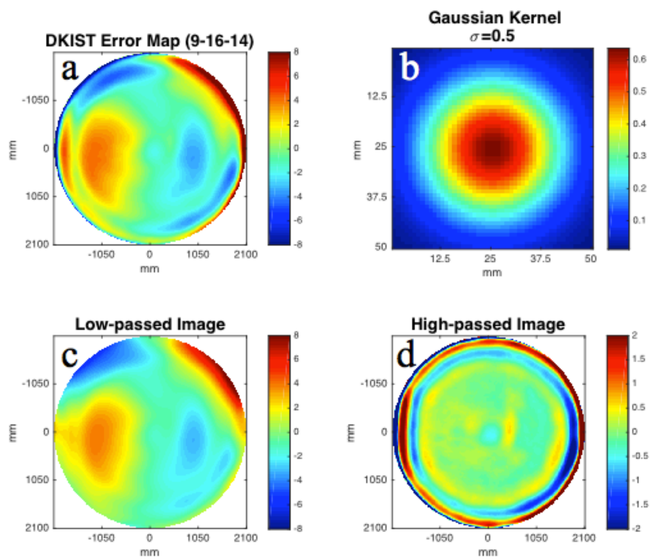

Figure 28 *Gaussian filter applied to DKIST error map 9/16/14. Unfiltered surface error map (a), gaussian kernel (50x50 mm) (b), low-pass filtered error map (c), high-pass filtered error map (d).*

Gaussian filtering is favorable in image processing for its ability to filter high-frequency noise, while preserving desirable high-frequency features , such as edge effects (Gonzalez, 2009). Traditional low-pass filters that define strict cut-off frequencies are susceptible towards unwanted frequency responses. The Fourier transform of the filter describes its frequency response, or influence in the spectral domain. The Fourier transform of a Gaussian is a Guassian, thus frequencies are influenced by the smooth trailing tail of the Guassian curve. The filter dominates as a low-pass filter, but still allows high frequencies to pass as function of how quickly the Gaussian tail decays. The 2-D Gaussian filter takes the form: $G(x, y) = \frac{1}{2\pi\sigma^2} e^{-\frac{x^2+y^2}{2\sigma^2}}$, where $\sigma$is the standard deviation, defining how quickly the tail decays, and x and y define the limits of the kernel.

5.0.2 XYProfile

XYProfile plots surface profiles along the x- and y-axes, for both *map* and *freqmap* datatypes. This module provides a quick look at surface features along these profiles, and allows the user to relate the surface height distribution to Zernike polynomials for aberration analysis. These plots also provide a tool for monitoring material removal over the progression of a grinding or polishing run set. This is useful to monitor surface figure as it converges to the nominal shape. The example displayed by Figure 29 (below) shows a surface map with z2 = 2 µm (tilt about y-axis) and z7 = 4 µm (vertical coma), and the corresponding profiles along the x- and y-axis. The example displayed by Figure 30 (below) shows a similar example, now with z7 = 4 µm (vertical coma) and z11 = 2 µm (spherical aberration) defining the surface figure.

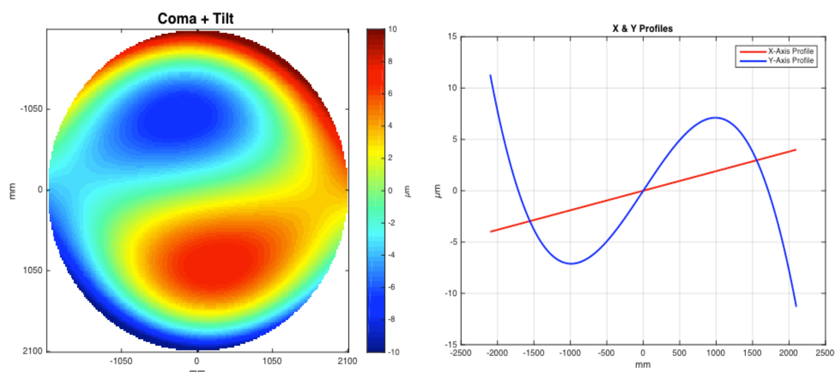

Figure 29 *2D Surface map z2 = 2µm, z7 = 4µm (left). Profiles along x and y-axes (right).*

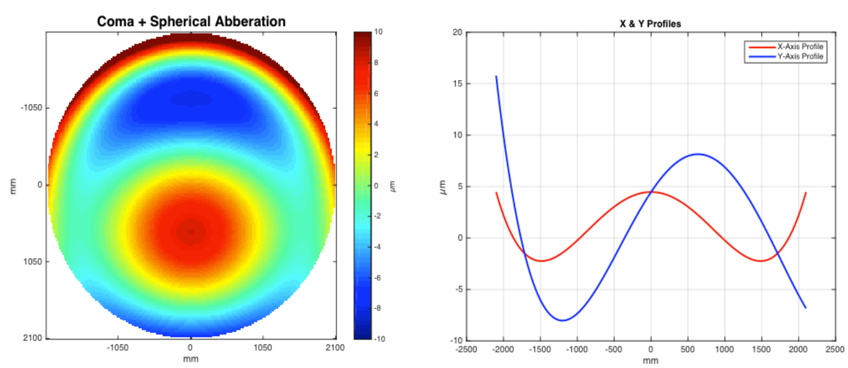

Figure 30 *2D Surface map z7 = 4µm, and z11 = 2µm (left). Profiles along x and y-axes (right).*

These profiles explicitly show the linear contribution of tilt, the cubic contribution from coma, and the quartic influence from spherical aberration. These examples show a simple demonstration on surface aberrations and their corresponding radial frequency, much like wavefan plots.

6.0 Macros

There are situations where multiple modules are needed to complete a single analysis. SAGUARO's macro builder allows multiple modules to run in a user specified order. Macros are then saved for recurring use. In one example, when applying a low-pass filter to a surface map, a total of five standard modules are needed for the resulting low-pass filtered map. First a Fourier transform is performed, using *MapFFT*, then a filter is applied to specify the cutoff frequency, using *FreqMap_LPFilter,* then an inverse Fourier transform is needed to regain spatial coordinates, using *FreqMap_IFFT,* then a circular mask is applied to hide artifacts from taking the Fourier transform of a rectangular matrix, using *MapMasktool*, and finally the resulting low-pass filtered image is plotted, using *MapPlot*. Building the macro is simple using the *SAGUARO Macro Editor*. Figure 31 (below) shows the *Macro Editor* with the five modules needed to achieve a complete low-pass filtered image. Figure 32 (below) shows the before and after surface maps as a product of the macro.

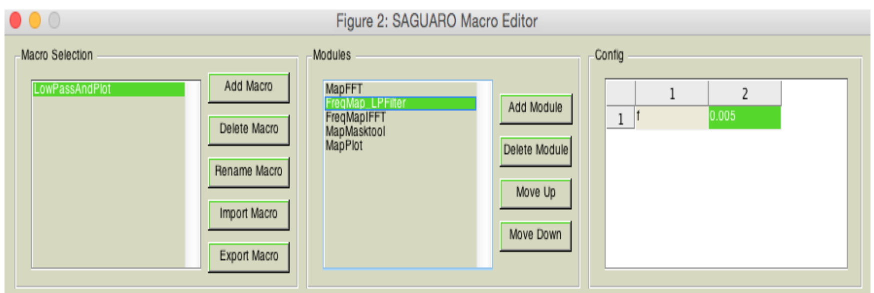

Figure 31 *SAGUARO Macro Editor showing example of a macro to perform a low-pass filtered image ,with cutoff frequency of 0.005 mm*$^{-1}$.

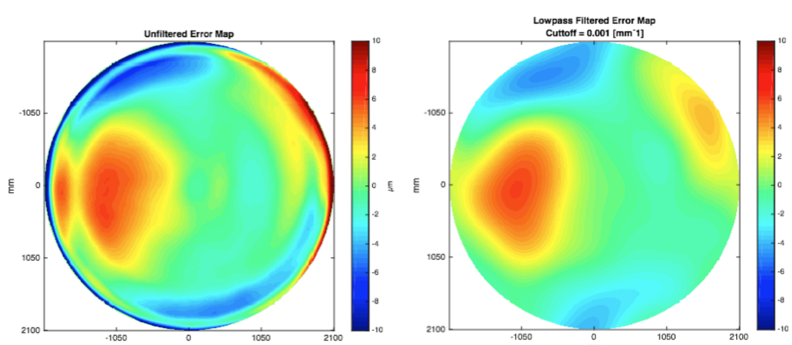

Figure 32 *Result from macro example, original surface map (left) and low-pass filtered surface map with cutoff frequency 0.005 mm*$^{-1}$.

7.0 Optical Metrology Application

7.1 DKIST Primary Mirror During Grinding Phase

The DKIST 4.2-m off-axis parabolic mirror was ground at the University of Arizona in 2014. Using SLOTS, five surface error maps were measured over a two-week grinding phase (shown below in Figure 33). This section of the report analyzes these five surface error maps exclusively using SAGUARO. Modules that are most applicable to optical fabrication and metrology are showcased. The analysis of the surface error maps gives insight on the progression of the surface error during the grinding phase. The following information is examined from the error maps; surface statistics, decomposition of Zernike polynomial coefficients for aberration quantification, Zernike term removal for aberration analysis, frequency filtering for spatial frequency analysis, profile plots for tracking surface smoothness, slope maps for analyzing high spatial frequency, and simulated interferograms for optical metrology.

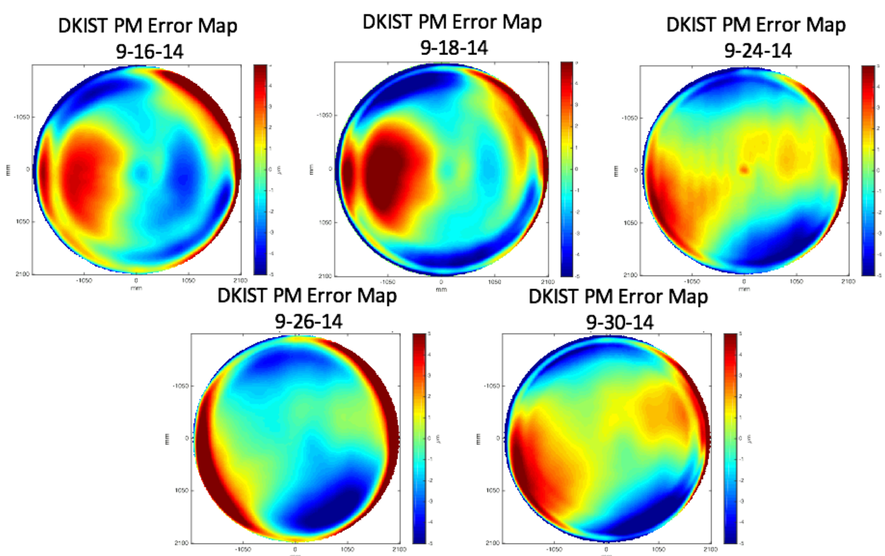

Figure 33 *Five DKIST primary mirror error maps over two-week span, measured using SLOTS.*

Before analyzing surface error, it is important to examine the nominal surface of which the error departs from. The mirror is decomposed into its aspheric components using the module *ZernikeTermRemoval*, see Figure 34 (below). It is useful to recognize the surface figure and magnitude of the aspheric departure, as surface error is directly related. It is common to grind aspheres in two steps. First the best-fit sphere is ground into the surface, and then aspheric departure is ground in. At the transition point, the error map will look very similar to the aspheric departure, with an inverted orientation. Recall that surface error maps shows the necessary removal needed to meet surface figure and surface finish specification. To retrieve the aspheric departure from the nominal surface, Zernike polynomials with zero angular frequency must be removed (i.e., defocus, low-order spherical aberration, and high-order spherical aberration). (See Figure 34 b below.) To analyze only high-order aspheric contribution, the first eight Zernike terms are removed (Kim et al, 2014). (See Figure 34 c below.)

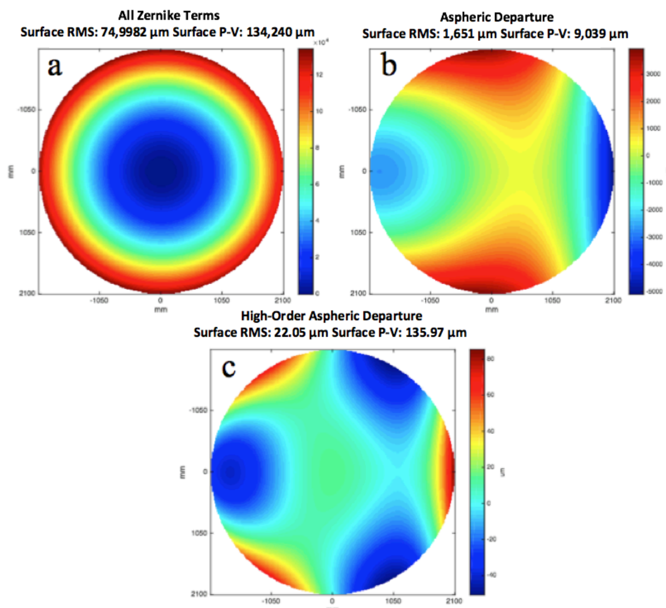

Figure 34 *Nominal surface of DKIST primary mirror (a). Aspheric departure of DKIST primary mirror, standard terms z1-z4, z11, and z22 removed (b). High-order aspheric departure in DKIST primary mirror, standard terms z1- z8 removed (c).*

Utilizing *MapStatistics* it is shown there is approximately 9-mm surface P-V of total aspheric departure across the 4.2-m mirror. High-order aspheric departure accounts for 0.135-mm P-V of the 9-mm total.

Grinding aspheres is much more difficult compared to traditional grinding of spherical surfaces, due to the challenging tools needed for grinding aspheres. The tooling used for grinding and polishing plays a crucial role in optical surfacing, as surface figure and finish are completely dependent on tooling. Tool misfit on an aspheric surface, with conic constant K, is related to the size of the tool lap with radius a, and the distance b from the asphere optical axis (Malacara, 2001), see Figure 35 (below).

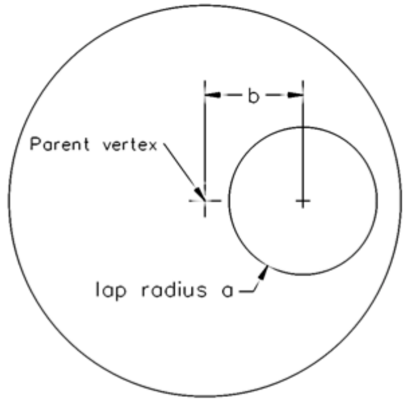

Figure 35 *The lap misfit is calculated for a polishing surface with diameter 2a, offset from the vertex of the parent asphere by an amount b. (Malacara, 2001).*

There are four common tooling parameters that contribute towards tool misfit, see Table 2 (below). The first describes tool misfit for a lap fitting a spherical surface, with defined radius *R.* The second describes tool misfit for a revolving lap about the optical axis. The third describes tool misfit as a function of tool rotation $\Delta\theta$**.** The fourth tooling parameter describes tool misfit through small translations in the lap, Δb, relating to tool stroke. Tooling misfit contributes to undesired features in surface error, and takes the form as optical aberrations, i.e., power, coma, astigmatism and spherical aberration. Power is defined by a radius of curvature mismatch. Astigmatism defines the difference in curvature along two specific axes. Coma defines misfit as a cubic function of lap size, and spherical aberration as a quartic function of lap size.

	Power	**Astigmatism**	**Coma**	**Spherical**
1.spherical lap	$\frac{Ka^4}{8R^3}+\frac{Ka^2b^2}{2R^3}$	$\frac{Ka^2b^2}{2R^3}$	$\frac{Ka^3b}{3R^3}$	$\frac{Ka^4}{32R^3}$
2.revolving lap	0	$\frac{Ka^2b^2}{R^3}$	$\frac{2Ka^3b}{3R^3}$	0
3. small rotation $\Delta\theta$	0	$\frac{Ka^2b^2}{R^3}\Delta\theta$	$\frac{Ka^3b}{3R^3}\Delta\theta$	0
4. small translation Δb	$\frac{Ka^2b}{R^3}\Delta b$	$\frac{Ka^2b}{R^3}\Delta b$	$\frac{Ka^3}{3R^3}\Delta b$	0

Table 2 *P-V lap misfit (Malacara, 2001).*

Table 2 (above) provides a tooling design guide for grinding and polishing aspheres. We notice that optimal tooling for reducing fitting error is achieved with a small tool, with a small stroke. There are tradeoffs associated with using small compliant tools and large rigid tools. Large rigid tools are able to remove more material in a shorter time, and provide good smoothing. Large rigid tools however are susceptible to misfit due to compliance, and may lose their desirable smoothing capabilities. Small compliant tools conform to the surface better, allowing for excellent tool fit for controlled figuring (Kim and Burge, 2010). Small tools however have the downside of long dwell times, as well as the inability to smooth over large areas, which makes them susceptible to creating high frequency zones. Aspheres require combinations of both types of tooling for the added benefits of each. Luckily for this mirror, the University of Arizona used their novel Stressed lap, to gain both tooling benefits.

For each surface error map, we can analyze the aberration composition using the *Map2Zernike* module. Table 3 (below) shows the first 11 standard Zernike coefficients corresponding to each error map.

z	**9/16/14 [μm]**	**9/18/14 [μm]**	**9/24/14 [μm]**	**9/26/14 [μm]**	**9/30/14 [μm]**
1	-1.05E-02	2.36E-02	2.18E-02	2.13E-02	2.33E-02
2	-4.95E-02	-8.55E-02	-5.58E-02	-5.34E-02	-5.79E-02
3	8.07E-04	5.05E-03	2.68E-03	4.82E-03	5.54E-03
4	2.42E-01	-7.56E-01	-2.93E-01	1.56E+00	-6.11E-01
5	1.41E+00	1.16E+00	1.23E+00	1.40E+00	1.59E+00
6	7.14E-01	1.50E+00	1.58E+00	1.78E+00	1.51E+00
7	4.67E-02	1.37E-01	-1.67E-01	-1.75E-01	-1.29E-01
8	1.88E+00	1.79E+00	6.51E-01	8.35E-01	7.55E-01
9	2.62E-01	2.23E-01	3.99E-02	-2.10E-02	-2.57E-03
10	-4.84E-01	-4.64E-01	2.90E-01	3.59E-01	3.85E-01
11	2.16E-01	-1.86E-01	4.31E-01	1.37E+00	-1.36E-01

Table 3 *First 11 standard Zernike terms for each error map.*

From Table 3 is it noticeable that the dominant aberrations are from terms z5, z6, z7, and z8, which correspond to low-order coma and astigmatism. We also notice that piston, tip, tilt, and defocus are contributing on a smaller scale. These aberrations, z1-z4, are induced during the measurement and may be removed. This is accomplished using SAGUARO's module *ZernikeTermRemoval*. Figure 36 (below) shows the DKIST surface error maps with z1-z4 removed.

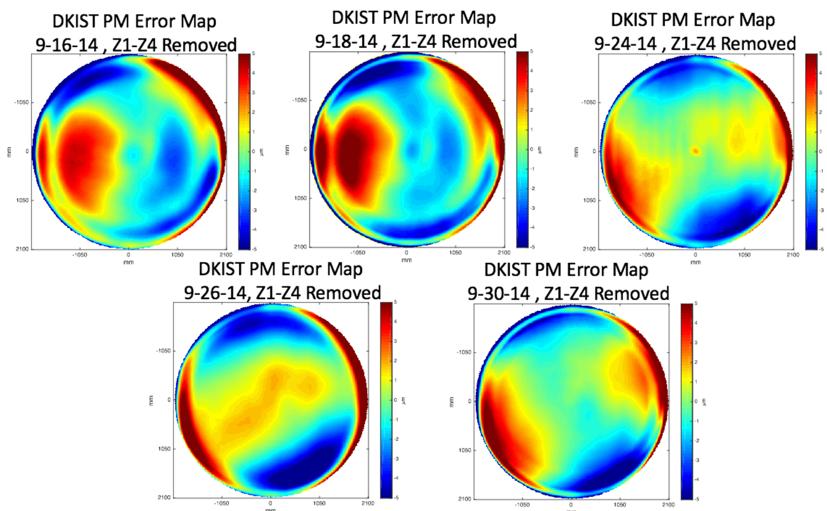

Figure 36 *DKIST surface error maps with piston/x-tilt/y-tilt/power removed.*

The transparency of other aberrations becomes more pronounced with z1-z4 eliminated. The maps qualitatively show dominating surface aberrations (see Appendix B for aberration surface plots). Referring to Figure 36 (above) the initial error map is dominated by a combination of coma and astigmatism. Coma is pronounced by cubic height dependence along a single axis, and astigmatism is pronounced by quadratic height dependence along two orthogonal axes. As time passes the comatic error is reduced, and astigmatism appears as the dominant error. Other high-order aberrations are present in these maps, but perhaps coma and astigmatism have more to say in the analysis? Using the module *Zernike2Map*, the astigmatism and coma Zernike coefficients, from Table 3 (above), are constructed into surface maps without any other aberration influence. These surfaces are plotted in Figure 37 (below).

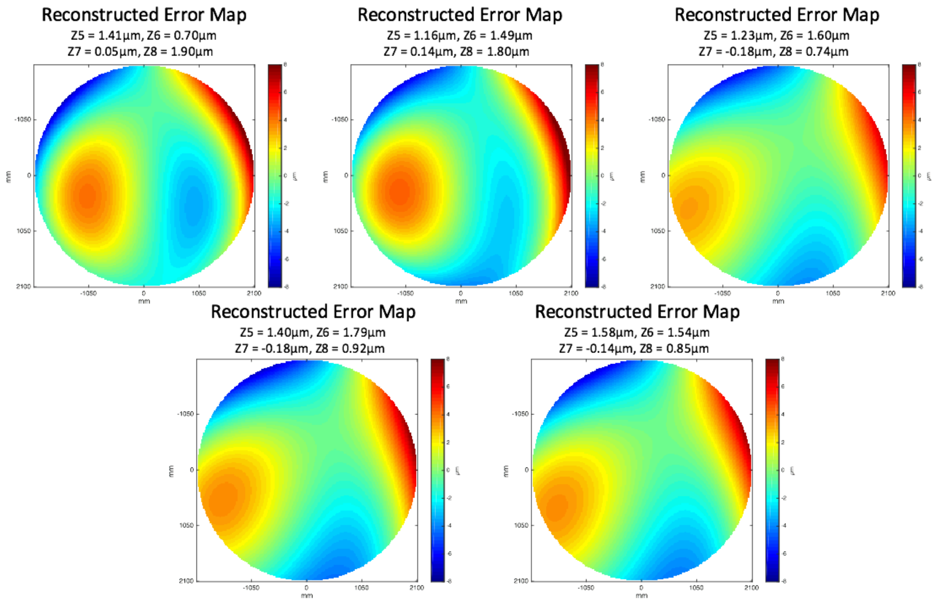

Figure 37 *Reconstructed DKIST surface error maps from Zernike terms z5-z8.*

As the error maps change surface figure over time, they begin to converge to a shape that approaches the nominal aspheric departure. Figure 38 (below) shows a comparison of the final error map, and the nominal aspheric departure. The error map shows where removal is needed, with red representing regions needing high removal. As the error map approaches the aspheric departure, it shows that grinding is effectively working towards correcting the surface figure. Once the surface figure is within a few handfuls of microns P-V, the mirror can begin polishing to target surface finish (Malacara, 2009). It is desirable to minimize surface error, which is only possible through a systematic approach. Understanding dominant surface aberrations allows for removal optimization through proper tooling and computer-controlled optical surfacing.

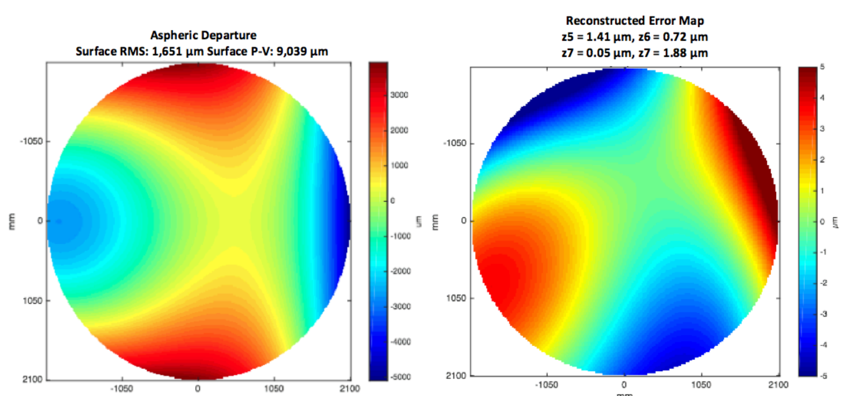

Figure 38 *Comparison of DKIST PM aspheric departure (left), to 9/30/14 reconstructed error map using z5-z8 (right).*

A quick approach to monitor error convergence is to track surface statistics after every grinding or polishing run. Surface rms, surface P-V, and slope magnitude rms can monitor surface figure and finish. Using SAGUARO's *MapStatistics* we can outline the following surface statistics over the five error maps, see Table 4 (below).

Date	**Surface rms [µm]**	**Surface P-V [µm]**	**Slope magnitude rms [µrad]**
9-16-14	2.9	37.9	28.5
9-18-14	3.2	43.2	67
9-24-14	2.6	37.8	27.4
9-26-14	3.2	37.3	25.7
9-30-14	2.8	43.4	35.9

Table 4 *Error map statistics, shown in surface rms, surface P-V and slope magnitude rms.*

Looking at the statistics in Table 4 (above) there appears to be no obvious convergence trend within any of the three categories. It may be the case that with such a large optic being ground, it can take several weeks or months of fine grinding to see these surface error statistics converge. The grinding phase is meant for gross removal, and initial shaping of the part towards its final figure. Gross removal can easily swing these statistics up and down as the grinding results in drastic change. It is more relevant to use these statistics to track error convergence once the part enters the polishing phase. In polishing, the surface slowly approaches the final figure and surface roughness, thus each statistic should show a slow convergence until the part has met specification. The specification is typically stated as a fraction of a specified wavelength, i.e. $\frac{\lambda}{5}, \frac{\lambda}{10}, \frac{\lambda}{20}$.

As previously discussed, tool misfit is a real and unavoidable challenge in optical surfacing. Tool misfit contributes undesirable surface error, or tooling artifacts. Common artifacts are sharp surface slopes, which create high spatial frequency zones in the optical surface. An appropriate metrology step is to monitor high and low frequency contributions to the optical surface. The SAGUARO module *HighPassLowPass* provides both high and low spatial frequencies of the error maps. High-pass filtered maps are shown in Figure 39 (below), as well as low-pass filtered maps in Figure 40 (below).

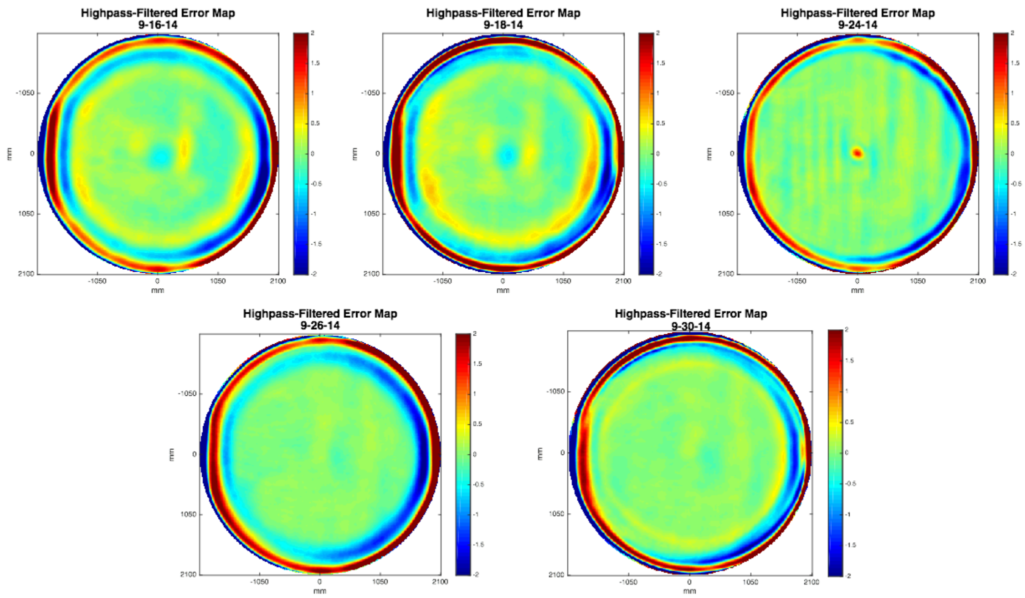

Figure 39 *High-pass filtered spatial frequency error maps.*

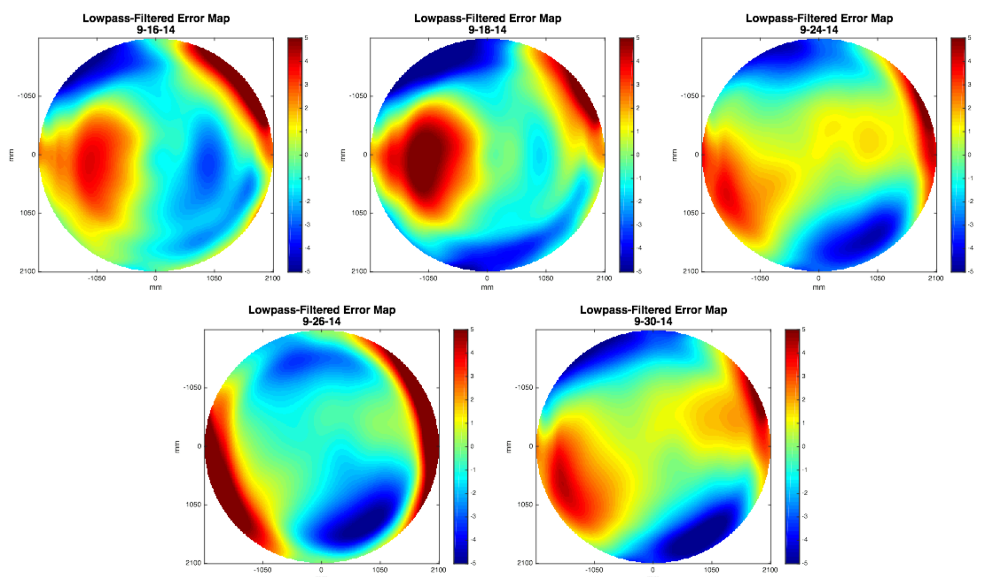

Figure 40 *Low-pass filtered spatial frequency error maps.*

The high-passed error maps contain ring-shaped figures, predominately along the edge of the part. These features are likely tooling artifacts caused from the difficultly of grinding near the edge. Grinding near the edge poses the risk of rolling the edge, and thus requires a very stiff tool to prevent this effect. Due to the risk, tools are limited, and proper fitting is difficult to achieve. This results in tool artifacts in the form of high spatial frequencies, or high-sloped regions. Monitoring surface slope errors shows the optical designer if a tool is misbehaving, allowing for modifications and corrections to the tool and surface. SAGUARO's *SurfaceStatistics* provides various slope maps. Figure 41 (below) shows the slope magnitude maps for each DKIST error map.

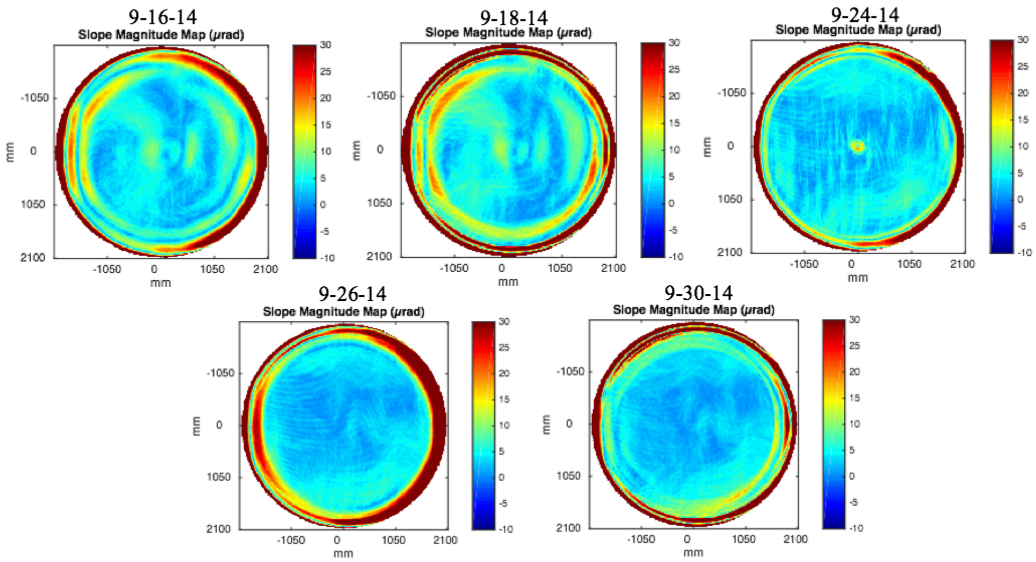

Figure 41 *Slope magnitude maps of DKIST surface error maps.*

Slope maps and high-pass filtered maps work hand in hand within identifying high-sloped regions. The high-pass filtered map provides a qualitative assessment of these regions, while the slope magnitude map provides the quantitative analysis, allowing a direct comparison to the slope specification.

The 2D surface map provides multiple ways of processing its data, however another desirable metrology step analyzes 1D surface profiles. A profile along a single axis can track removal and provide insight into the surface error. Profiles along the x- and y-axes can be monitored for asymmetric error maps, and radially averaged profiles are desirable for symmetrical error maps. One example may include polishing a radial zone for an extended period of time, say along the edge of the surface for smoothing high frequencies. Here, the radially averaged profile is a great method to track smoothing and removal. The SAGUARO modules *XYProfiles* and *RadiallyAvg2Coords* provide these plots, and are shown in Figures 42 (below).

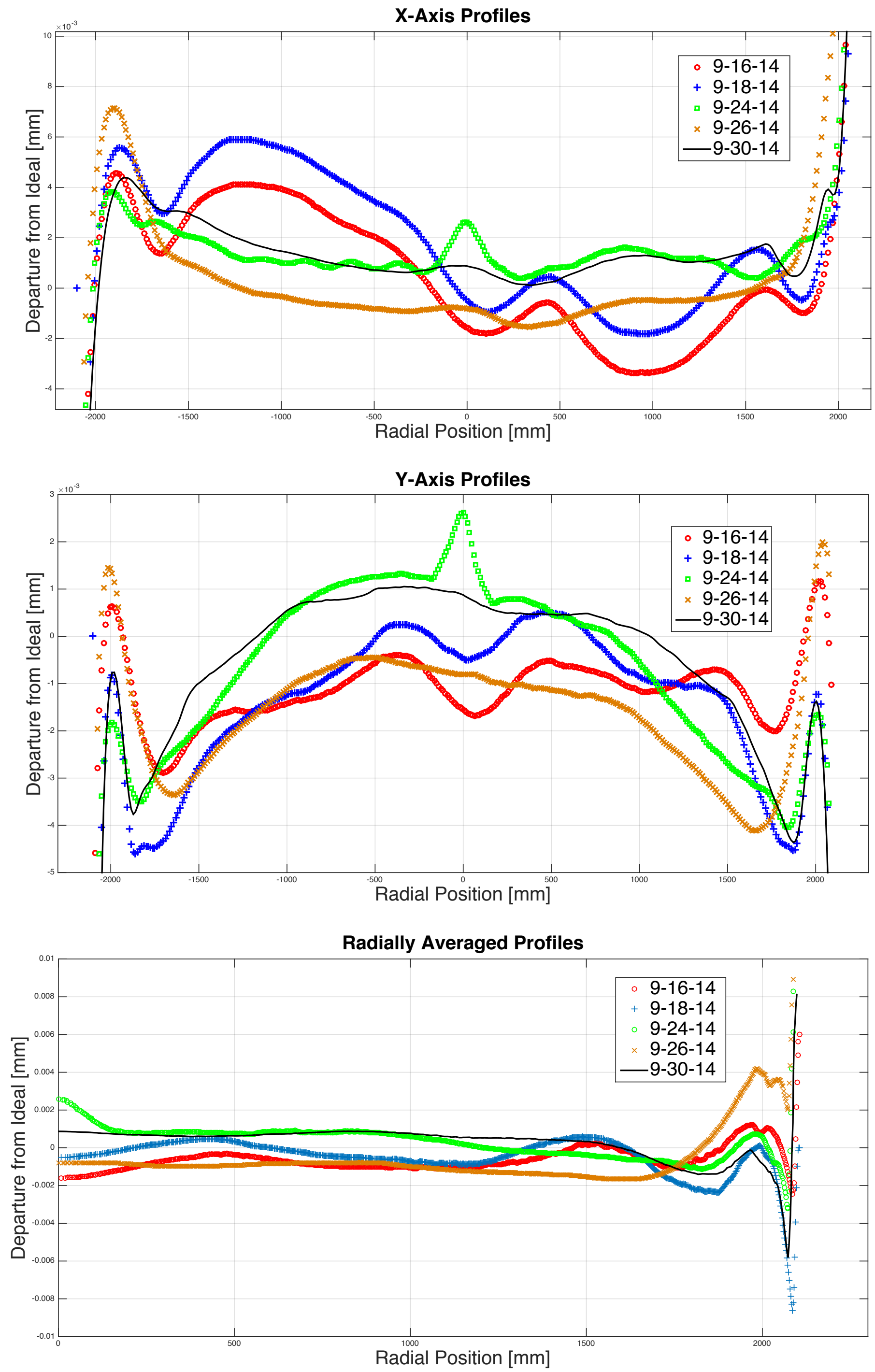

Figure 42 *Profile analysis over the five error maps, x-axis profile (top), y-axis profile (middle), radially averaged profile (bottom).*

Even though these profiles do not thoroughly characterize the part, they contribute a meaningful analysis. Each graph exhibits the same trend, showing that the error is continually smoothed over time, excluding the edge effects. This is shown through the small variance in the latest error profile (9/30/14), compared to its predecessors. These graphs also provide insight on the high-sloped edge, specifically showing how the edge has been shaped over time and the resulting changes in slope. These plots can be used as a template for creating tools that properly fit the sharp edge characteristics, i.e. full sized ring tools.

An appropriate analysis to conclude with, simulates optical interferograms of the error maps. Simulating an interferogram gives an idea of what the surface will look like under an interferometric optical test. Testing with an interferometer provides the most accurate depiction of the part, and is often used to quote the final part specifications. There are high risks involved when large optics are relocated from their polishing home to a separate testing location. In this scenario it is only practical to make the relocation when it is certain that the optical surface will produce useable fringe data. The module *ApplyArbitraryFunction* allows the cosine of the data to be taken, providing a reasonable estimation of the fringe patterns when simulated under interferometric test. Surface height error $H(x, y)$ is related to phase by $\phi(x, y) = \frac{4\pi}{\lambda} * H(x, y)$, where λ corresponds to the wavelength of the interferometer used under testing (Wyant et al, 2006). The interferogram is simulated by converting each pixel to phase, and then taking the cosine to observe relative phase shifts. Figure 43 (below) shows simulated interferograms for each error map, using λ=0.6328 µm.

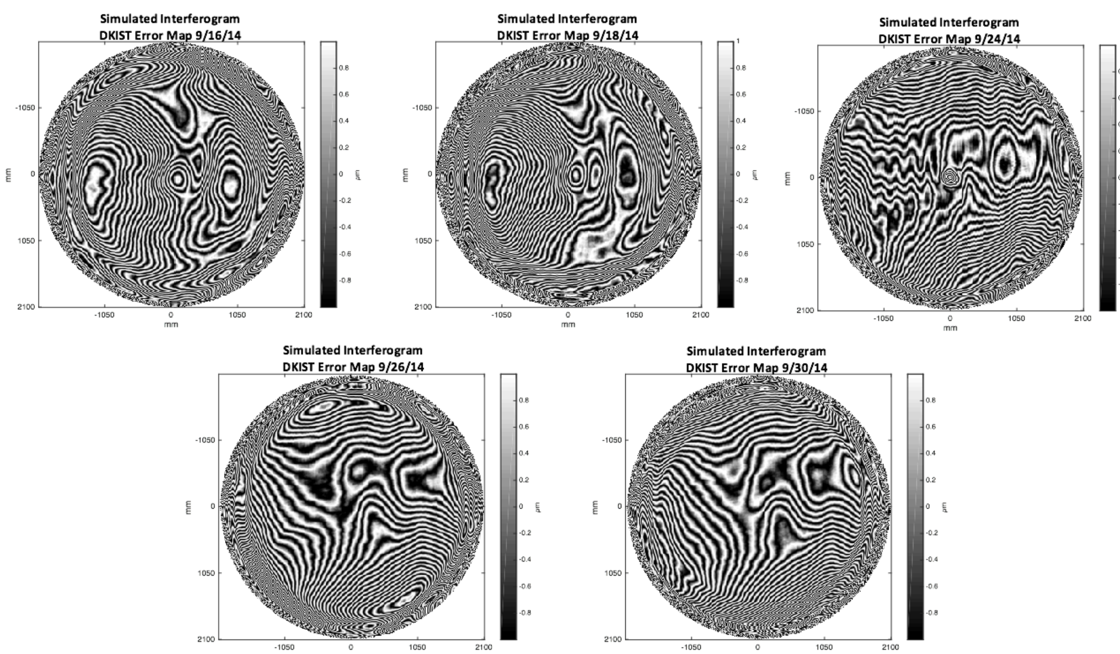

Figure 43 *Simulated interferograms of DKIST error maps.*

The simulated interferograms show partially resolvable fringes throughout the center areas; however high frequency fringes are present along the edges of the part, corresponding to high-sloped regions. It is concluded from the simulations that this mirror is not ready for an optical test, due to the large annular regions showing unresolvable fringes. This result is expected due to the current grinding stage of the optic. Nonetheless this module shows its functionality towards the appropriate application.

7.2 Concluding Remarks

This application has shown that with a handful of modules from SAGUARO, a variety of processing is accomplished to aide with optical metrology. The processed data gives optical engineers and opticians information to optimize their next step forward with grinding and polishing, whether computer-controlled or not. Tracking the progression of error maps is critical for identifying anticipated trends as well as adverse trends. Error maps should always be converging in some aspect toward the final figure.

As shown in this example, surface error does not obviously converge by solely monitoring surface rms, surface P-V, or slope magnitude rms. These statistics have no noticeable trend of convergence, and even show raised P-V and slope magnitude values after two weeks of grinding. In this situation figure of merit cannot be accessed from these statistics, but rather qualitatively analyzed through other means. Spatial frequency filtering and profile analysis shows that the error progressively smooths over the majority of the part, however with difficulties near the edge. The battle of blending the edge with the rest of the part creates high and sharp features. As the error reduces in magnitude over the majority of the part, the edge effectively grows much larger in height, which may explain the growth in surface P-V over the two weeks. Likewise, as the slopes are smoothed over the majority of the part, but the edge becomes higher and sharper, the slope magnitude rms is increased. If the edge effects are excluded from the figure of merit, it is reasonable to state that the surface error is converging. This is evident from smoothing shown in each profile plot as well as the low-passed spatial frequency maps. There is also evident progression shown in the reduction of coma, which brings the surface closer to its nominal shape. The remaining error over two-weeks of grinding is around 40 μm P-V, consisting of mostly astigmatism, of which follows closely in shape to the aspheric departure.

The SLOTS measurement technique has proved to supply a sequence of data of which conclusions can be differentiated. The measurements show high resolution of the finely ground surface, allowing for precise statistical analysis as well as qualitative analysis. SAGUARO provides a platform for verifying the fidelity of the measuring device, through processing of the data taken with the device. Optical designers can feel confident designing grinding runs based off the accuracy of SLOTS, and can utilize SAGUARO as a convenient data processing platform.

Appendix A - Zemax Zernike Polynomial Notation

The most general way to represent the Zernike polynomials is in the form

$$R_n^m(\rho)e^{im\theta} = \begin{cases} R_n^m(\rho)\cos m\theta \\ R_n^m(\rho)\sin m\theta \end{cases}$$

The radial portion of the polynomial is defined by two indices, n and m. The n index defines the order of the radial power, while the m index defines the azimuthal order. Only certain values for m are allowed once n is chosen; n + m must be even. The terms are orthonormal such that the magnitude of the coefficient of each term is the rms contribution of the term. The first 11 terms are listed in the below table.

z	**m**	**n**	Z_n^m
1	0	0	1
2	1	1	$\sqrt{4}\rho cos\phi$
3	-1	1	$\sqrt{4}\rho sin\phi$
4	0	2	$\sqrt{3}(2\rho^2 - 1)$
5	-2	2	$\sqrt{6}(\rho^2 sin2\phi)$
6	2	2	$\sqrt{6}(\rho^2 cos2\phi)$
7	-1	3	$\sqrt{8}(3\rho^3 - 2\rho)sin\phi$
8	1	3	$\sqrt{8}(3\rho^3 - 2\rho)cos\phi$
9	-3	3	$\sqrt{8}\rho^3 sin3\phi$
10	3	3	$\sqrt{8}\rho^3 cos3\phi$
11	0	4	$\sqrt{5}(6\rho^4 - 6\rho^2 + 1)$

Table 5 *Relating SAGUARO Zernike coefficients to Zernike Polynomials*

Appendix B - Zernike Surface Plots

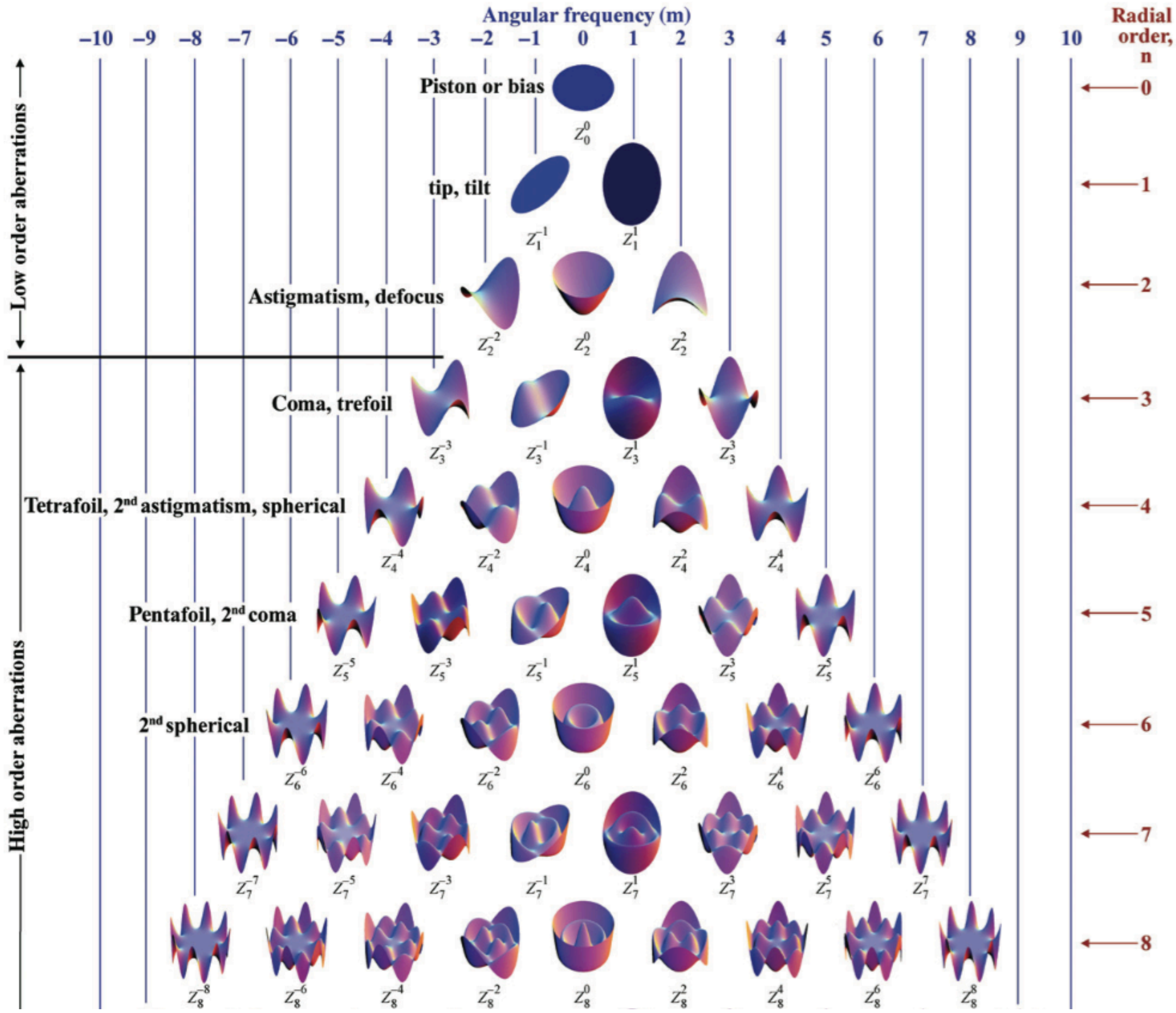

Figure 44 Surface plots of the Zernike polynomial sequence up to 8 orders. (Fleck et al., 2011)

References

Dae Wook Kim and James H. Burge, "Rigid conformal polishing tool using non-linear visco-elastic effect," Opt. Express 18, 2242-2257 (2010)

D. W. Kim, C. J. Oh, P. Su, and J. H. Burge, "Advanced Technology Solar Telescope 4.2 m Off-axis Primary Mirror Fabrication," in *Classical Optics 2014*, OSA Technical Digest (online) (Optical Society of America, 2014), paper OTh2B.3.

Erkin Sidick, *Power spectral density specification and analysis of large optical surfaces.* Proc. SPIE 7390, Modeling Aspects in Optical Metrology II, 73900L (June 15, 2009); doi:10.1117/12.823844.

Gonzalez RC, Woods RE; *Digital image processing* (3rd ed.). J. Biomed. Opt. 0001;14(2):029901-029901-2.

Goodwin, E. P., Wyant, J. C., & Society of Photo-optical Instrumentation Engineers. (2006). *Field guide to interferometric optical testing*. Bellingham, Wash. (1000 20th St. Bellingham WA 98225-6705 USA): SPIE.

Kim, Dae Wook. (2015) *Accurate and rapid IR metrology for the manufacture of freeform optics*. SPIE Newsroom. DOI: 10.1117/2.1201506.006015

Lyons, R. G., 1948. (2011).*Understanding digital signal processing* (3rd ed.). Upper Saddle River, NJ: Prentice Hall.

Malacara, D., 1937, & Wiley InterScience (Online service). (2007). *Optical shop testing* (3rd ed.). Hoboken, N.J: Wiley-Interscience.

Malacara, D., 1937, & Thompson, B. J. (2001). *Handbook of optical engineering*. New York: Marcel Dekker.

Rao, K. Ramamohan (Kamisetty Ramamohan), Kim, D. N., & Hwang, J. J. (2010). *Fast fourier transform: Algorithms and applications*. Dordrecht;New York;: Springer.

Ross Zhelem; *Specification of optical surface accuracy using the structure function*. Proc. SPIE 8083, Modeling Aspects in Optical Metrology III, 808310 (May 23, 2011); doi:10.1117/12.889143.

Vasudevan Lakshminarayanan & Andre Fleck (2011) *Zernike polynomials: a guide, Journal of Modern Optics*, 58:7, 545-561, DOI: 10.1080/09500340.2011.554896